03
2020

BILINGUAL PUBLISHING CO.
Pioneer of Global Academics Since 1984

Volume 3 | Issue 3 | July 2020 | ISSN 2630-5119 (Online)

Journal of Atmospheric Science Research

ISSN 2630-5119
03
9 772630 511201

Volume 3 Issue 3 • July 2020 • ISSN 2630-5119 (Online)

Journal of Atmospheric Science Research

BILINGUAL PUBLISHING CO.

Pioneer of Global Academics Since 1984

BILINGUAL PUBLISHING CO.
Pioneer of Global Academics Since 1984

Volume 3 | Issue 3 | July2020 | Page1-40
Journal of Atmospheric Science Research

Contents

ARTICLE

REVIEW

BILINGUAL PUBLISHING CO.
Pioneer of Global Academics Since 1984

Journal of Atmospheric Science Research
https://ojs.bilpublishing.com/index.php/jasr

ARTICLE

Absence of the Impact of the Flux of Cosmic Rays and the Cloud Cover on the Energy Balance of the Earth

H. I. Abdussamatov*

Pulkovo Observatory of the RAS, St. Petersburg, 196140, Russia

ARTICLE INFO

Article history
Received: 13 July 2020
Accepted: 22 July 2020
Published Online: 30 July 2020

Keywords:
Climate; Cosmic rays
Cloud Cover
Energy Balance
Little Ice Age
Solar Irradiance
Greenhouse Effect
Atmospheric Transparency Window

ABSTRACT

The energy of solar radiation absorbed by the Earth, as well as the thermal radiation of the Earth's surface, which is released to the space through the atmospheric transparency window, depends on variations of the area of the cloud cover. Svensmark et al. suggest that the increase in the area of the cloud cover in the lower atmosphere, presumably caused by an increase in the flux of galactic cosmic rays during the quasi-bicentennial minimum of solar activity, results only in an increase in the fraction of the solar radiation reflected back to the space and weakens the flux of the solar radiation that reached the Earth surface. It is suggested, without any corresponding calculations of the variations of the average annual energy balance of the Earth *E*, that the consequences will include only a deficit of the solar energy absorbed by the Earth and a cooling of the climate up to the onset of the Little Ice Age. These suggestions ignore simultaneous impact of the opposite aspects of the increase in the area of the cloud cover on the climate warming. The latter will result from a decrease in the power of thermal radiation of the Earth's surface released to the space, and also in the power of the solar radiation reflected from the Earth's surface, due to the increase in their absorption and reflection back to the surface. A substantial strengthening in the greenhouse effect and the narrowing of the atmospheric transparency window will also occur. Here, we estimate the impact of all aspects of possible long-term 2% growth of the cloud cover area in the lower atmosphere by *E*. We found that an increase in the cloud cover area in the lower atmosphere will result simultaneously both in the decrease and in the increase in the temperature, which will virtually compensate each other, while the energy balance of the Earth E before and after the increase in the cloud cover area by 2% will stay essentially the same: $E_1 - E_0 \approx 0$.

1. Introduction

Determination of the physical mechanism of the global climate variation is one of the most important problems. The Earth climate is a complex non-linear system subject to the impact of numerous factors, dynamical parameters and cause-and-effect feedback. The climatic system depends on an extremely complicated set of long-term (about 30 years and more) physical processes in the "ocean - ground - atmosphere" system, and these processes, in turn, are susceptible to various, primarily quasi- bicentennial

**Corresponding Author:*
H. I. Abdussamatov,
Pulkovo Observatory of the RAS, St. Petersburg, 196140, Russia;
Email: abduss@gaoran.ru

 DOI: https://doi.org/10.30564/jasr.v3i3.2129

variations in the total solar irradiance (TSI). If we take into account only quasi-bicentennial variations in TSI equal to ~0.3% [1,2], the resulting increments in the planetary temperature will be small (~0.2 K). However, these variations are very important as a triggering mechanism for subsequent numerous feedback effects, which result in considerable variations in Bond albedo of the Earth, abundance of greenhouse gases in the atmosphere, and the absorption within atmospheric transparency windows [3-6]. The solar radiation energy absorbed by the Earth, as well as the thermal radiation of the Earth's surface released to the space through the transparency window, depends on variations of the area and optical density of the cloud cover and the parameters of the underlying terrain. The stability of the climate is determined by the long-term equilibrium state of the annual average energy balance of the Earth between the TSI inflow into the outer layers of the atmosphere and the total radiation exhausted from the Earth atmosphere to the space in all directions (Figure 1). However, representative long-term data for deviations of the annual average energy balance of the Earth from the state of equilibrium, regardless of their reasons, are of fundamental importance for determination of the regular patterns of climatic variations and climate forecasts. A vital factor that undoubtedly affects the Earth climate is quasi-bicentennial variations of the TSI. Two aspects should be mentioned here: TSI variations and variations in the solar activity. Experimental data indicate that TSI varies synchronously and correlate both in the phase and in the amplitude with 11-year and quasi-bicentennial cycles of the solar activity [4,5].

2. The Average Annual Energy Balance of the Earth

The energy balance of the Earth E is specified in the outer layers of the atmosphere (Figure 1) as the annual average difference between the power per unit area of TSI inflow and that of escaping thermal radiation and both reflected and scattered fractions of TSI, determined by Bond albedo:

$$E = \frac{\left(S_{\odot} + \Delta S_{\odot}\right)}{4} - \frac{(A_{\mathrm{BE}} + \Delta A_{\mathrm{BE}})\left(S_{\odot} + \Delta S_{\odot}\right)}{4} - \varepsilon\sigma(T_p + \Delta T_p)^4, \quad (1)$$

where $S_{\odot}$ is TSI, $\Delta S_{\odot}$ the TSI increment, A_{BE} the Earth's global albedo (Bond albedo), ΔA_{BE} the increment of the Bond albedo, ε the irradiating capacity of the surface-atmosphere system, σ the Stefan-Boltzmann constant, T_p the planetary thermodynamic temperature, ΔT_p the increment of the planetary thermodynamic temperature, E the power-per-unit-area variations of the heat content of the planet. The planetary thermodynamical temperature is the average temperature over the total surface of the planet (the surface of the Earth and the atmosphere).

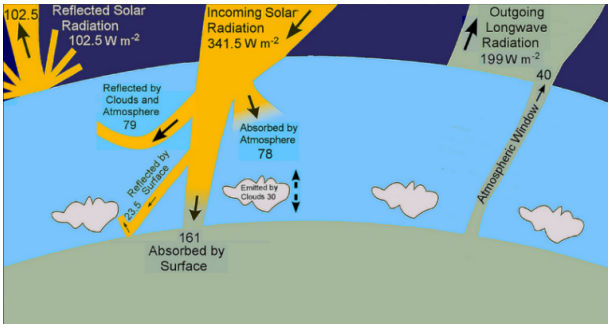

Figure 1. Average annual values of all components in the total energy balance of the Earth as a planet at the outer atmospheric layers in an equilibrium state [3,5,7,8]

Svensmark et al. [9-12] suggest that the increase in the cloud cover area in the lower atmosphere of the Earth presumably caused by the impact of the increasing flux of galactic cosmic rays in the period of the quasi-bicentennial deep minimum of the solar activity results only in an increase in the reflected fraction of the solar radiation inflow and therefore weakens the flux of the solar radiation that reaches the Earth's surface. Presenting no calculations of the variations of the energy balance of the Earth, these authors suggest that this will inevitably result in the deficiency of the solar energy absorbed by the Earth and in the global cooling up to the onset of a Little Ice Age. Along with that, they totally ignore simultaneous impact of opposite aspects of the increase in the area and the optical density of the cloud cover on the climate warming. The above occurs through the following factors: a decrease in the outflowing thermal radiation of the Earth's surface and the solar radiation reflected from the Earth's surface, due to an increase in their absorption and reflection back towards the surface; a significant strengthening of the greenhouse effect and narrowing of the atmospheric transparency window. The authors explain the onset of the global warming by a decrease in the flux of the cosmic rays and decrease in the cloud formation rate, which results in a growth in the absorbed fraction of the solar radiation within the time of the Grand maximum of the solar activity. They also totally ignore simultaneous direct influence of parallel TSI decrease by ~0.3% [1,2] within the framework of quasi-bicentennial cycle on the variation in the energy balance of the Earth and subsequent variations of physical processes in the atmosphere caused by secondary feedback effects. Such a long-term energy imbalance between the Earth and the space, caused by the decrease in TSI by ~0.3% ($\Delta S_{\odot} \approx 4$ w/m^2), taking into account thermal inertia will inevitably result in the subsequent steady decrease in the temperature (without taking into account other contributions and for at

DOI: https://doi.org/10.30564/jasr.v3i3.2129

immutability of Bond albedo $\Delta A_{BE} = 0$) by

$$\Delta T_e = \frac{\Delta S_{\odot}(1 - A_{\mathrm{BE}} - \Delta A_{\mathrm{BE}}) - \Delta A_{\mathrm{BE}} S_{\odot}}{16\sigma T_e^3} \approx -0.2\ \mathrm{K}. \qquad (2)$$

3. The Spectral Density of Thermal Radiation of the Earth's Surface

Under the current conditions, carbon dioxide and water vapor absorb about 80% of the thermal radiation of the Earth's surface. Out of these, ~68% is absorbed in spectral bands of the basic greenhouse gas - the water vapor, and only ~12% by the carbon dioxide (Figure 2). This ratio is caused by partial overlapping of spectral absorption bands of the carbon dioxide and the water vapor, and also by virtually constant abundance of water vapor in the atmosphere within small variations of the temperature and pressure. If it were not for the overlap of these spectral absorption bands, the water vapor would absorb ~77% of the thermal radiation of the Earth's surface, while the carbon dioxide only ~17%. With their current approximately stable area and optical density, the clouds along with molecules of other minor greenhouse gases absorb another ~10% of the thermal radiation of the Earth's surface, and the remaining ~10% are released to the outer space through the transparency windows of the Earth's atmosphere. Both the fraction of the thermal radiation of the surface released to the outer space, and that absorbed by cloudiness belong to virtually the same broad bands of the spectral wavelengths (Figure 2).

Due to the growth of the cloud cover area, both absorbed and reflected (towards the surface) energy of the thermal radiation of the surface increases within the wavelength range of the transparency windows of the atmosphere. As a result, the energy of non-absorbed thermal radiation of the Earth's surface, released to the outer space within the spectral intervals of the transparency windows, will respectively decrease by virtually the same value. Consequently, the carrying capacity (transparency) of the atmosphere with respect of the release of the thermal radiation of the Earth's surface to the outer space depends in particular of variation of the fraction of the thermal radiation of the Earth's surface absorbed and reflected by the clouds. As a rule, Bond albedo, the width of the transparency windows of the atmosphere, and the carrying capacity of the atmosphere with respect to thermal radiation of the Earth's surface released into the outer space reach their maximum values within long-term periods of deep cooling and decrease to their minimum values at the stage of global warming. Concentration of greenhouse gases in the atmosphere varies inversely.

4. Climatic Effects of Possible Cloud Coverage Variations

The area and optical density of the cloud cover is a basic part of the annual average energy balance of the Earth. Any physical process that may result in their noticeable systematic variations presents big interest. In particular, variations in the area and optical density of the cloud cover affect the fraction power of both the inflowed solar radiation absorbed by the Earth and thermal radiation of the Earth's surface released to the outer space through the transparency windows of the atmosphere. A possible growth of the optical density and area of the cloud cover increases the part of the inflow of the solar radiation reflected back to the space, thereby weakening the flux of solar radiation that reaches the Earth's surface. According to the hypothesis [9-12], this possible growth in the area of the cloudiness will result only in a corresponding deficiency in the inflowed solar energy and a long-term negative annual average energy balance of the Earth. This hypothesis states that the reflecting effect of the increase in cloudiness, additionally weakening the solar radiation, will inevitably result in cooling of the climate up to a Little Ice Age. The same hypothesis also explains the global warming by a decrease in the flux of cosmic rays and lowering of cloud formation rate, which result in an increase in absorbed fraction of the solar radiation within the time of a high maximum of the solar activity. It is extremely important to estimate whether the suggested negative balance of the annual average energy budget of the Earth (due to the increase in the flux of cosmic rays and the cloud cover) will be significant and whether its impact can play a noticeable role in the subsequent cooling and the onset of the Little Ice Age in the time of the forthcoming Grand Minimum of the solar activity [3-6,13]. For the first time, we carried out a combined estimate of oppositely directed previously unknown aspects of an increase in the area and optical density of the cloud cover. They simultaneously increase both the absorption and reflection of thermal radiation of the Earth's surface and the solar radiation reflected from the Earth's surface back to the surface, and also the greenhouse effect. They also result in narrowing of the atmospheric transparency windows through which thermal radiation of the Earth's surface is released to the outer space. They present an important reservoir of accumulation of heat energy, which virtually compensate the cooling caused by the increase in the part of the TSI inflow reflected back to space.

In spite of the current uncertainty in the degree of the impact of the increase in the flux of cosmic rays on the considerable growth of the cloud cover area, on the annual

 DOI: https://doi.org/10.30564/jasr.v3i3.2129

balance of the average energy budget of the Earth and on the subsequent cooling of the climate [14-16], for the first time we will attempt to estimate another unexplored and oppositely directed aspect of the influence of the growth in the cloud cover area on the climate. The increase in the area and optical density of the cloud cover simultaneously result also in inevitable increase in the absorption and reflection of thermal radiation of the surface, and also the solar radiation reflected from the surface. Consequently, they lead to direct air heating and to the formation of supplementary energy in the atmosphere, which finally results in an increase in the temperature of the atmosphere due to effective narrowing of the transparency windows of the atmosphere. In addition, the increase in the area and optical density of the cloud cover in the lower atmosphere results in strengthening of the greenhouse effect, which will also add up to the heating of the atmosphere and the planet in total. The resulting supplementary energy is radiated by the heated atmosphere, both to the space and, through the inverse radiation, on the surface, which is heated. Therefore, it is very important to determine the degree and the role of the oppositely directed influence of the growth in the area and optical density of the cloud cover on the annual average energy balance of the Earth and on subsequent heating processes. This determination will make it possible to specify the influence of the growth in the area and optical density of the cloud cover also in the opposite processes of global variation in annual average energy balance of the Earth and the climate. To this end, thorough their research are needed.

Here, we will restrict our consideration with the analysis and estimate of the efficiency of the impact of the possible long-term increase in the area and optical density of the cloud cover during the Grand Minimum of the solar activity simultaneously both on the increase in the reflected part of the inflowing solar radiation back to the outer space and on the growth in absorption and reflection of the thermal radiation of the surface, and also on the solar radiation reflected from the surface. We will also consider their combined oppositely directed impacts on the variation of the balance of the annual average energy budget of the Earth and the subsequent global variation of the climate. Due to the increase in the area and optical density of the cloud cover, the absorbed and reflected (towards the surface) energy of the thermal radiation of the surface increases within a broad wavelength range of spectral bands in the transparency windows of the atmosphere (Figure 2). As a result, the energy of non-absorbed thermal radiation of the Earth's surface, released to the space within the transparency windows of the atmosphere, will decrease virtually by the corresponding value, due to the decrease in the transparency windows of the atmosphere, while the atmosphere itself will gain the absorbed energy. As a result, in the case of long-term increase in the area and optical density of the cloud cover, the atmosphere will effectively display supplementary absorbed energy, which was not released to the space due to the narrowing of the transparency windows of the atmosphere. For the first time, we fully extended and revised estimated the long-term impact of all aspects of possible 2% growth in the cloud cover area in the lower atmosphere on the current annual average energy balance of the Earth E_o. These factors result particularly in the narrowing of the atmosphere transparency window for the release of the radiation of the Earth's surface and also both in the energy deficiency and in the accumulation of supplementary heating energy [17].

Let us try to estimate a possible variation of the current annual average energy balance of the Earth E_o, if the cloud cover area in the lower atmosphere of the Earth will experience a long-term consistent 2% growth, presumably caused by an increase in the flux of galactic cosmic rays. In this case, the fraction of incoming solar radiation reflected from the clouds back to the space (≈79 W/m^2) will also increase roughly by 2%. This will weaken the flux of solar radiation that reaches surface layers and will result in a decrease in E_o by about -0.02 x 79 W/m^2 = -1.58 W/m^2 and in corresponding cooling.

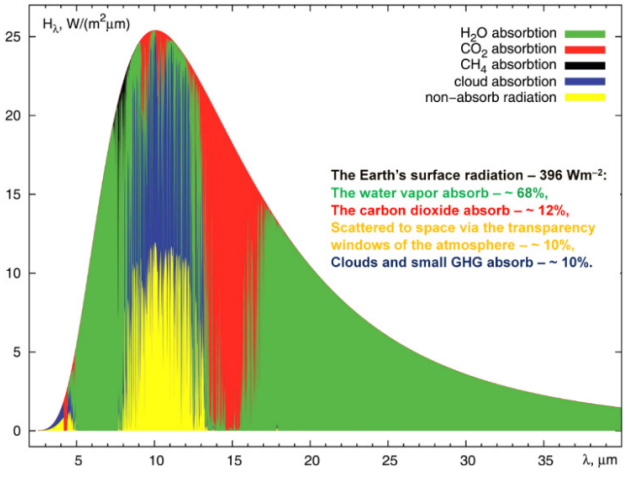

Figure 2. Spectral density of the thermal long-wave radiation flux from the surface of the Earth (as black-body) [4,5].

However, at the same time, with the increase in the cloud cover area, the energy of thermal radiation of the Earth's surface absorbed by clouds increases by some 2%, while the a energy released to space through the transparency windows of the atmosphere (≈ 40 W/m^2) will respectively decrease. This factor increases the flux of energy in surface under cloud layers and will result in

DOI: https://doi.org/10.30564/jasr.v3i3.2129

some warming and in an increase in E_o by about +0.02 x 40 W/m^2 = +0.8 W/m^2. At the same time, a fraction of the solar radiation reflected from the surface of the Earth and released to space (≈23.5 W/m^2), will also decrease, since its reflection by clouds in the direction of the surface will increase by some 2%. This will result in an increase in E_o roughly by +0.02 x 23.5 W/m^2 = +0.47 W/m^2 and in air heating under the clouds and above the surface. Simultaneously, thermal radiation of the surface of the Earth absorbed and reflected back to the surface by the cloud cover will fare increases roughly by 2%; the same is true for the absorption and reflection of the solar radiation (back to the surface) reflected from the Earth's surface. They will result in some heating of the air between the clouds and the surface and in an increase in *Eo* by +**X.XX W/m^2**. Besides, the increase in the cloud covers in the lower layers of the atmosphere substantially strengthens the greenhouse effect, which also results in a noticeable increase in E_o by +**Y.YY W/m^2** with subsequent heating. The radiation ejected from the clouds (≈30 W/m^2) will increase in 2% both in the direction of the space and in the direction of the Earth's surface. This will lead to a decrease in E_o by approximately -0.02 x 30 W/m^2 = -0.6 W/m^2 and to some cooling. Simultaneously, this will also result in an increase in E_o by roughly +0.02 x 30 W/m^2 = +0.6 W/m^2 and in some warming. The calculations provide a new energy balance of the Earth after an increase in cloud cover area by 2% $E_1 \approx E_o$ - 1.58 W/m^2 + 0.8 W/m^2 + 0.47 W/m^2 - 0.6 W/m^2 + 0.6 W/m^2 + **X.XX W/m^2 + Y.YY W/m^2.** Hence, $\Delta E = E_1 - E_o \approx 0$, i.e. the difference between energy balance of the Earth before and after the increase in the cloud cover area is virtually equal to zero [8,17]. Consequently, the impact of the increase in the cloud cover area, presumably caused by the influence of galactic cosmic rays, on the climate is virtually no-existent. Thereby, a long-term increase in the cloud cover presumably caused by the influence of the increase in the flux of cosmic rays, virtually does not result in variation in the annual average energy balance of the Earth, i.e. essentially does not affect variation of the climate.

5. Conclusions

The increase in the cloud cover area presumably resulted from an increase in the flux of galactic cosmic rays in the time of a deep minimum of the solar activity simultaneously leads to both negative energy balance of the planet, through the increase in reflection of the solar radiation back to space, and in the positive balance, increasing the absorption and reflection of the thermal radiation of the Earth's surface, strengthening the greenhouse effect and narrowing the transparency window of the atmosphere, which compensate the energy losses and cooling. A possible increase in the area and optical density of the cloud cover with the increase of the flux of galactic cosmic rays virtually does not result in violations of the energy balance of the Earth and does not affect the variations of the climate.

Note in addition that according to Clausius-Clapeyron ratio, cooling results in an decrease in vaporization from the World Ocean and the terrain and in the lowering of the abundance of water vapor in the atmosphere. Consequently, the atmosphere will contain less water vapor, which in turn will decrease the formation of clouds and the total area of cloud cover. Global terrestrial climate is determined exceptionally by long-term (for time periods about 30 years and more) variations of the global thermal state (heat content) of the total planet, which is specified by its annual average global energy balance, restricted by excess or deficiency of the difference between the absorbed planet fraction of the inflowing solar energy and the intrinsic thermal energy radiated by the Earth and released to the outer space; this is combined with no less important subsequent numerous impacts of cause-and-effect feedbacks. Influence of oppositely directed aspects of the possible increase in the cloud cover virtually compensate the cooling caused by the growth in the fraction of the inflowing solar radiation reflected back to space.

It is known that very insignificant long-term variations in annual average TSI related to long-term cyclical variations in the shape of the Earth's orbit (the so-called Milankovitch cycles) and combined with subsequent very important (due to long-term variations in the TSI and temperature) non-linear feedback effects, result in Grand Ice Ages (with the period of about 100,000 years) and sequential glacial and interglacial cycles [5,18]. These Grand Ice Ages, with appreciably larger temperature in ~10-12°C drops (practically an order of magnitude more) occur cyclically and independently of any large long-term variations of solar activity, cosmic rays and cloudiness. From the above we can conclude that the increases in the flux of cosmic rays and in cloud cover and the subsequent climate cooling are virtually unrelated and that the hypothesis of the dominating role of the cosmic rays flux in the deep climate cooling up to a Little Ice Age is scientifically unsound. The warming of Mars and virtually of the entire Solar system in the last quarter of the XX century [19,20] also does not confirm the influence of the growth in the cosmic rays flux on variations of the climate compared to the influence of TSI variations observed in the quasi-bi-centennial solar cycle [1,2,4,5,13]. Thereby the climatic sensitivity to the increase in the cosmic rays flux

 DOI: https://doi.org/10.30564/jasr.v3i3.2129

within the Grand minimum of solar activity, supposedly resulting in the increase in area and optical density of the cloud cover, is virtually nonexistent. Therefore, we cannot expect for any real substantial decrease in the temperature of the Earth, leaving alone an onset of a Little Ice Age, caused by a possible effect of the growth in the flux of galactic cosmic rays presumably resulting in an increase in the area and optical density of the cloud cover. Temperature trends of the Earth are dominated by quasi- bicentennial variability of TSI.

As a result, an impact of the long-term growth in the cloud cover area (presumably caused by an influence of an increase in the cosmic rays flux) on variations in the annual average energy budget of the Earth and, consequently, on the climate is virtually nonexistent. The increases in the energy of the radiation emitted by clouds with larger area to the outer space and towards the surface of the Earth are roughly equal, and virtually do not affect the energy balance of the Earth, i.e., the thermal radiation of the clouds does not affect variations in the energy balance of the planet.

Thereby, variations in the cloud cover area caused presumably by the impact of galactic cosmic rays virtually do not result in any climatic effects. The Earth climate does not depend on variations of cosmic rays and the cloud cover and is determined only by long-term variations in energy imbalances between the Earth and the space, as well as subsequent numerous feedback effects.

Acknowledgments

This study was partly supported by the Project No. KP19-270 of the Praesidium of the Russian Academy of Sciences for Fundamental Scientific Research ("Issues of the Origin and Evolution of the Universe Using Methods of Ground-Based Observations and Space Research").

References

[1] Shapiro, A. I., Schmutz, W., Rozanov, E., Schoell, M., Haberreiter, M., Shapiro, A. V., Nyeki, S. E. A new approach to the long-term reconstruction of the solar irradiance leads to large historical solar forcing / Astron. Astrophys. 2011, 529: A67.

[2] Egorova, T., Schmutz, W., Rozanov, E., Shapiro, A. I., Usoskin, I., Beer, J., Tagirov, R. V., Peter, T. Revised historical solar irradiance forcing / Astron. Astrophys. 2018, 615: A85.

[3] Abdussamatov, H. I. Lunnaya observatoriya dlya issledovanii klimata Zemli v epokhu glubokogo pokholodaniya (Lunar Observatory for Earth climate studies in the deep Ice Age) St. Petersburg: Nauka, 2017: 128. (In Russian)

[4] Abdussamatov, H. I. Current long-term negative average annual energy balance of the Earth leads to the new Little Ice Age / Thermal Sci. 2015, 19: S279-S288.

[5] Abdussamatov, H. I. The new Little Ice Age has started. Evidence-Based Climate Science. Easterbrook D. J. (ed) Oxford: Elsevier, 2016: 307-328.

[6] Abdussamatov, H. I. Comparative analysis of errors in monitoring the Earth's global energy budget by the Lunar Observatory and orbiters / Izv., Atmos. Ocean. Phys., 2018, 54(9): 1341-1352.

[7] Trenberth, K. E., Fasullo, J. T., Kiehl, J. Earth's global energy budget // Bull. Am. Meteorol. Soc., 2009, 90: 311-323. https://doi.org/10.1175/2008BAMS2634.1

[8] Abdussamatov, H. I. The Earth's climate does not depend on variations in cosmic rays and cloud coverage // Geomagnetism and Aeronomy. 2019, 59: 935-941.

[9] Svensmark, H., Friis-Christensen, E. Variation of cosmic ray flux and global cloud coverage - a missing link in solar-climate relationships / J. Atmos. Sol.-Terr. Phys. 1997, 59: 1225-1232. https://doi.org/10.1016/S1364-6826(97)00001-1

[10] Svensmark, H. Cosmoclimatology: A new theory emerges / Astron. Geophys. 2007, 48: 1.18-1.24. https://doi.org/10.1111/j.1468-4004.2007.48118.x

[11] Svensmark, H., Enghoff, M. B., Shaviv, N. J., Svensmark, J. Increased ionization supports growth of aerosols into cloud condensation nuclei / Nat. Commun. 2017, 8: 2199. https://doi.org/10.1038/s41467-017-02082-2

[12] Stozhkov, Y. I., Bazilevskaya, G. A., Makhmutov, V. S., Svirzhevsky, N. S., Svirzhevskaya, A. K., Logachev, V. I., Okhlopkov V. P. Cosmic rays, solar activity, and changes in the Earth's climate / Bull. Russ. Acad. Sci.: Phys. 2017, 81: 252-254.

[13] Nils-Axel, M. The approaching new Grand solar minimum and Little Ice Age climate conditions / Nat. Sci. 2015, 7: 510-518.

[14] Sloan, T., Wofendale, A. W. Testing the proposed causal link between cosmic rays and cloud cover // Environ. Res. Lett., 2008, 3(2): 024001. https://doi.org/10.1088/1748-9326/3/2/024001

[15] Sloan, T., Wofendale, A. W. The contribution of cosmic rays to global warming / J. Atmos. Sol.-Terr. Phys., 2011, 73(16): 2352-2355. https://doi.org/10.1016/j.jastp.2011.07.013

[16] Erlykin, A. D., Sloan, T., Wofendale, A. W. A review of the relevance of the 'CLOUD' results and other recent observations to the possible effect of cosmic rays on the terrestrial climate // Meteorol. Atmos. Phys., 2013, 121(3-4): 137-143.

DOI: https://doi.org/10.30564/jasr.v3i3.2129

https://doi.org/10.1007/s00703-013-0260-x

[17] Abdussamatov, H. I. Cosmic rays and clouds variations effect on the climate is insignificantly // Applied Physics Research. 2018, 10: 81-86.

[18] Milankovitch, M. Kanon der erdbestrahlungen und seine anwendung auf das eiszeitenproblem. In: Canon of insolation and the Ice Age problem. With Introduction and biographical essay by Nikola Pantic. Hardbound Alven Global Belgrade, 1998: 636. (in English).

[19] Odyssey studies changing weather and climate on Mars. The changing south polar cap of Mars: 1999-2005, MGS MOC Release. 2005(MOC2-1151).

[20] Ravilious, K. Mars melt hints at solar, not human, cause for warming, scientist says. National Geographic News, 2016.

 DOI: https://doi.org/10.30564/jasr.v3i3.2129

BILINGUAL PUBLISHING CO.
Pioneer of Global Academics Since 1984

Journal of Atmospheric Science Research
https://ojs.bilpublishing.com/index.php/jasr

ARTICLE

Cyclone Bomb Hits Southern Brazil in 2020

Ricardo Gobato1* Alireza Heidari[2]

1. Green Land Landscaping and Gardening, Seedling Growth Laboratory, 86130-000, Parana, Brazil
2. Faculty of Chemistry, California South University, 14731 Comet St. Irvine, CA 92604, USA

ARTICLE INFO

Article history
Received: 16 July 2020
Accepted: 28 July 2020
Published Online: 30 July 2020

Keywords:
Atmospheric phenomenon
Cyclone Bomb; Brazil
Chapecó
Extratropical cyclone
Parana
Santa Catarina
Rio Grande do Sul
Santa Catarina
Winter

ABSTRACT

An "explosive extratropical cyclone" is an atmospheric phenomenon that occurs when there is a very rapid drop in central atmospheric pressure. This phenomenon, with its characteristic of rapidly lowering the pressure in its interior, generates very intense winds and for this reason it is called explosive cyclone, bomb cyclone. With gusts recorded of 116 km/h, atmospheric phenomenon - "cyclone bomb" (CB) hit southern Brazil on June 30, the beginning of winter 2020, causing destruction in its influence over. One of the cities most affected was Chapecó, west of the state of Santa Catarina. The satellite images show that the CB generated a low pressure (976 mbar) inside it, generating two atmospheric currents that moved at high speed. In a northwest-southeast direction, Bolivia and Paraguay, crossing the states of Parana and Santa Catarina, and this draft that hit the south of Brazil, which caused the destruction of the affected states. Another moving to Argentina, southwest-northeast direction, due to high area of high pressure (1022 mbar). Both enhanced the phenomenon.

1. Introduction

With winds of 100 km h "explosive extratropical cyclone" [1] left a trail of destruction in Santa Catarina, Paraná and Rio Grande do Sul on Tuesday, June 30, 2020. The phenomenon known as the "cyclone bomb" caused heavy rains, where gusts of wind destroyed houses, caused tree falls, debris and the destruction of the energy network.

The cyclone that hit the state on June 30, which reached 168.8 km/h in the most affected regions. The winds will calm down and the last days of the week will be marked by cold and dry weather, with sun during the day and the possibility of frost [2].

1.1 Weather News and Warnings

According to the Civil Defense of the southern states of Brazil, ten deaths were recorded [1]. Nine deaths occurred in Santa Catarina, the most affected state, and at least one person is missing in the municipality of Brusque. Another fatal victim in Rio Grande do Sul.

Based on the use of American and European numerical models, which simulate the atmosphere, the center

**Corresponding Author:*
Ricardo Gobato,
Green Land Landscaping and Gardening, Seedling Growth Laboratory, 86130-000, Parana, Brazil;
Email: ricardogobato@hotmail.com; ricardogobato@gardener.com

DOI: https://doi.org/10.30564/jasr.v3i3.2163

detected the formation of the CB near the south-Brazilian coast and to which an alert was sent to the states [1].

A rare climatic phenomenon will happen between Tuesday and Wednesday and will cause heavy rain with an incidence of winds with intensities above normal even for storms. Caused by the drop in atmospheric pressure, the phenomenon will attract polar air and cause the minimum temperature to fall below 5°C, especially at dawn on Wednesday. Tuesday's winds, which could reach 100 km/h in isolated bursts, could cause damage such as fallen trees, debris and damage to the electricity supply. On Wednesday the wind stops and the cold and humidity remain at work. On Thursday the polar air gets reinforced and on Friday the minimum should be one of the most bays of the year so far and can stay at around 3°C [3].

1.2 Cyclone Bomb (CB)

The occurrence of cyclones is relatively common for the region at this time of year, but the recent phenomenon has been exacerbated by other meteorological and atmospheric factors [1].

According to L. Calvetti, head of the Center for Meteorological Forecasting and Research at the Federal University of Pelotas (Ufpel), the so-called "explosive extratropical cyclone" occurs when there is a very rapid drop in central atmospheric pressure. Based on the use of American and European numerical models, which simulate the atmosphere, the center detected the formation of the CB near the south-Brazilian coast and to which an alert was sent to the states [1].

This phenomenon, with this feature to lower the pressure inside quickly generates very strong winds and so that name of explosive cyclones [1,4].

Information released by Rio Grande Energy and the State Electricity Company of Rio Grande do Sul, indicate that, in total, 639 thousand people were without power in the state. Already the Fire Department of Santa Catarina totaled more than 1,600 occurrences attended in the last 24 hours, post-phenomenon. For large-scale occurs, the tropical cyclones influence and are influenced by the weather and other atmospheric phenomena point of view, the call synoptic condition. A very intense circulation of heat and humidity from the North region, with emphasis on the Amazon and Bolivia, increased the occurrence of the cyclone more sharply, reaching Paraguay, Uruguay and northern Argentina, as well as the south-Brazilian coast [1].

Figure 1. Picture of the destruction caused by the cyclone pump in an urban area of the county of Chapecó in Santa Catarina, which is one of the hardest hit [1]. Photo: Chapecó City Hall (SC)

Figure 2. Santa Catarina State was the most affected by the cyclone; On image, area registration destroyed in Chapecó [1]. Photo: Chapecó City Hall (SC)

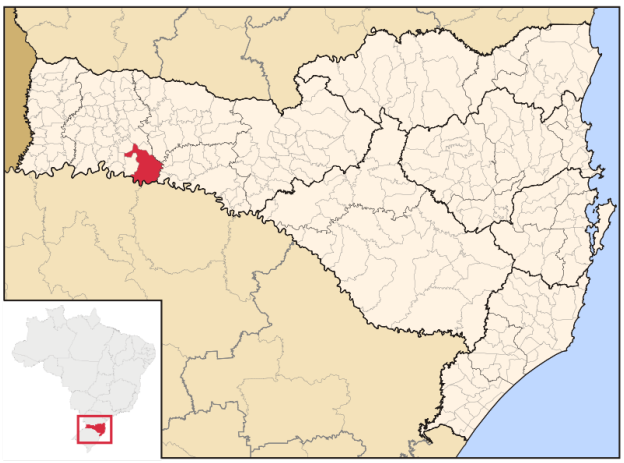

Figure 3. Map with the location of the County of Chapecó, west of the state of Santa Catarina [5].

The Chapecó located 27°06'17"S 52°36'51"W [6], the

 DOI: https://doi.org/10.30564/jasr.v3i3.2163

Figures (1-3) was the most affected by cyclone.

2. Theoretical Foundation

2.1 Tropical Cyclones

Tropical cyclones are stronger versions of tropical storms. They are intense circular storms that originate over warm tropical oceans and are characterized by low atmospheric pressure, high winds, and heavy rain. Drawing energy from the sea surface and maintaining its strength as long as it remains over warm water, a tropical cyclone generates winds that exceed 119 km (74 miles) per hour. In extreme cases winds may exceed 240 km (150 miles) per hour, and gusts may surpass 320 km (200 miles) per hour. Accompanying these strong winds are torrential rains and a devastating phenomenon known as the storm surge, an elevation of the sea surface that can reach 6 m (20 feet) above normal levels. Such a combination of high winds and water makes cyclones a serious hazard for coastal areas in tropical and subtropical areas of the world. Every year during the late summer months (July-September in the Northern Hemisphere and January-March in the Southern Hemisphere), cyclones strike regions as far apart as the Gulf Coast of North America, northwestern Australia, and eastern India and Bangladesh [4].

Tropical cyclones are known by various names in different parts of the world. In the North Atlantic Ocean and the eastern North Pacific they are called hurricanes, and in the western North Pacific around the Philippines, Japan, and China the storms are referred to as typhoons [4].

In the western South Pacific and Indian Ocean they are variously referred to as severe tropical cyclones, tropical cyclones, or simply cyclones. All these different names refer to the same type of storm [4].

2.1 The Anatomy of a Cyclone

Tropical cyclones are compact, circular storms, generally some 320 km (200 miles) in diameter, whose winds swirl around a central region of low atmospheric pressure. The winds are driven by this low-pressure core and by the rotation of the Earth, which deflects the path of the wind through a phenomenon known as the Coriolis force. As a result, tropical cyclones rotate in a counterclockwise (or cyclonic) direction in the Northern Hemisphere and in a clockwise (or anticyclonic) direction in the Southern Hemisphere [4-13].

The wind field of a tropical cyclone may be divided into three regions. First is a ring-shaped outer region, typically having an outer radius of about 160 km (100 miles) and an inner radius of about 30 to 50 km (20 to 30 miles). In this region the winds increase uniformly in speed toward the centre. Wind speeds attain their maximum value at the second region, the eyewall, which is typically 15 to 30 km (10 to 20 miles) from the centre of the storm. The eyewall in turn surrounds the interior region, called the eye, where wind speeds decrease rapidly and the air is often calm. These main structural regions are described in greater detail below [4-13].

3. Analysis of Satellite Images and Synoptic Charts of CB

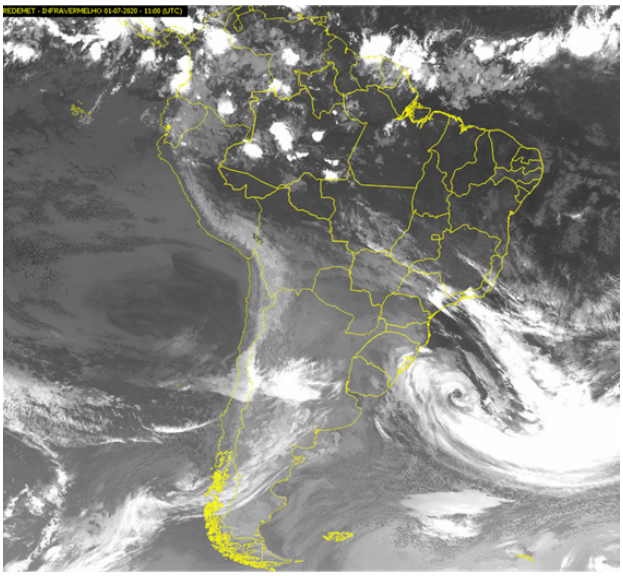

Figure 4. Image of the "bomb cliclone" moving to the Atlantic Ocean. Image in the infrared spectrum, July 1, 2020, 11:00 UTC. REDEMET [6,7]

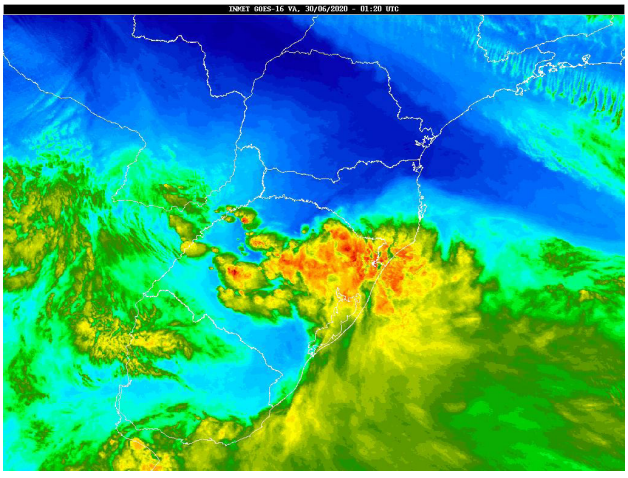

Figure 5. Enhanced image obtained by GOES-16 satellite, from June 30, 2020, at 01h20 UTC [3,5,14]

DOI: https://doi.org/10.30564/jasr.v3i3.2163

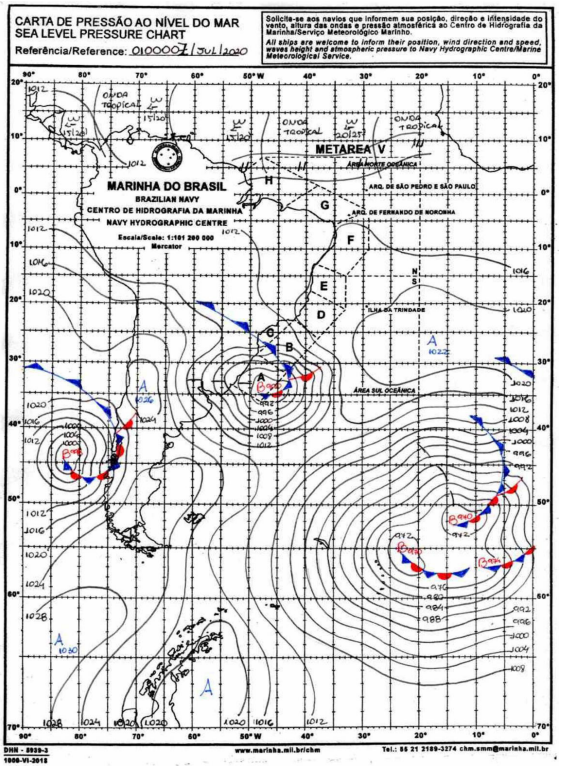

Figure 6. Synoptic Letters, from July 1, 2020, at 00h00 UTC. Navy Hydrography Center. Brazil's navy. Synoptic Letters [15]

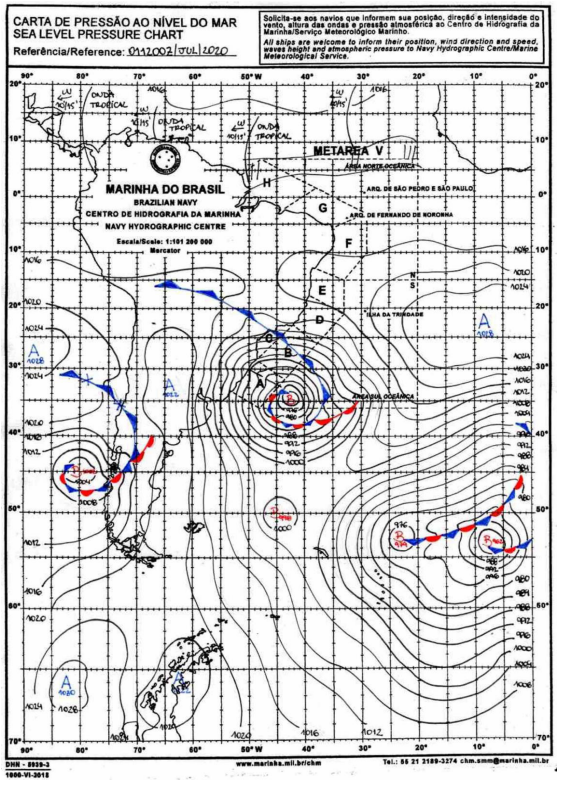

Figure 7. Synoptic Letters, from July 1, 2020, at 12h00 UTC. Navy Hydrography Center. Brazil's navy. Synoptic Letters [15]

The Figures (1-3) was the most affected by cyclone. The Chapecó located 27°06'17"S 52°36'51"W [6].

Figure (4) shows an image in the infrared spectrum of the cyclone moving towards the high seas, that is, the Atlantic Ocean. The eye of the cyclone is crisp, and gains intensity when advancing towards the ocean. Image of the "bomb cliclone" moving to the Atlantic Ocean., July 1, 2020, 11:00 UTC.

In Figure (5) enhanced image obtained by GOES-16 satellite, from June 30, 2020, at 01h20 UTC. In the dark blue color, an atmospheric current travels from Paraguay and Mato Grosso do Sul, crossed the states of Parana and Santa Catarina, going into shock with current coming from Argentina.

The synoptic chart Figure (6) shows a low pressure center of 990 mbar, with coordinates 35ºS 45°W, near the coast of Uruguay and Rio Grande do Sul, at 01:00 UTC on July 1, 2020.

A high pressure area 1026 mbar, over Argentina coordinates 35°S 70°W, moving in the direction to Paraguay. The synoptic chart in Figure (7) shows a 976 mbar low pressure center, coordinates 35ºS 40°W, next to Uruguay and Rio Grande do Sul coast, but away from the coast, 12:00 UTC on July 1, 2020.

The formation of the CB is clear, in Figures (4) and (7). An area of high pressure of 1022 mbar, over Argentina, with coordinates 35°S 65°W, continuing its movement towards Paraguay, acquiring greater amplitude and intensity.

4. Conclusion

The occurrence of cyclones is relatively common for the southern region of Brazil at this time of year, that is, winter, but the recent phenomenon is augmented by other meteorological and atmospheric factors.

CB generated a strong low pressure in its interior, creating two air streams which have worsened the phenomenon. An atmospheric current moved at high speed, in northwest-southeast direction, Bolivia, Paraguay, through the Paraná and Santa Catarina, and this airflow that hit the south of Brazil causing destruction. Another one traveled through Argentina in a southwest-northeast direction, colliding with the draft from Bolivia and Paraguay. Both of them clashed over the three southern states of Brazil. Only the outer edge of the CB reached the coast of the three states in the southern region of Brazil, Paraná, Santa Catarina and Rio Grande do Sul.

References

[1] L. Sudré. Saiba o que é o ciclone bomba que atingiu

o Sul e quais serão os impactos no Sudeste. Brasil de Fato. São Paulo (SP), 2020. URL: https://www.brasildefato.com.br/2020/07/01/saiba-o-que-e-o-ciclone-bomba-que-atingiu-o-sul-e-quais-serao-os-impactos-no-sudeste.

[2] L. Farias. Ciclone extratropical atingirá Oeste e Sul de Santa Catarina nesta terça-feira. NOTISUL, 2020. Available in: July 10, 2020. URL: https://notisul.com.br/geral/ciclone-extratropical-atingira-oeste-e-sul-de-santa-catarina-nesta-terca-feira/

[3] Ciclone extratropical trará chuva e ventos fortes nesta terça-feira. Tudo Online Campo Bom. Tudo Online em Campo Bom. Available in: July 11, 2020. URL: http://www.tudoonlineemcampobom.com.br/ciclone-extratropical-trara-chuva-e-ventos-fortes-nesta-terca-feira/.

[4] John P. Rafferty. Storms, Violent Winds, and Earth's Atmosphere. Series: Dynamic Earth. Britannica Educational Publishing, Year: 2010. ISBN: 1615301143,9781615301140,1615301887,9781615301881

[5] Chapecó. Creative Commons. CC BY-SA 3.0. https://creativecommons.org/licenses/by-sa/3.0/ Available in: July 11, 2020. URL: https://en.wikipedia.org/wiki/Chapec%C3%B3

[6] REDEMET. Rede de Meteorologia do Comando da Aeronáutica, 2020: GT-REDEMET, Imagens de Satélite, Available in: July 15, 2018, URL: https://www.redemet.aer.mil.br/index.php?i=produtosHYPERLINK «https://www.redemet.aer.mil.br/index.php?i=produtos&p=imagens-de-satelite»&HYPERLINK «https://www.redemet.aer.mil.br/index.php?i=produtos&p=imagens-de-satelite»p=imagens-de-satelite

[7] Krasny, R. A study of singularity formation in a vortex sheet by the point vortex approximation, J. Fluid Mech. 1986, 167: 65-93.

[8] P. G. Saffman. Vortex dynamics. Series: Cambridge monographs on mechanics and applied mathematics. First Edition, Cambridge University Press, 1992.

[9] M. A. Sokolovskiy, J. Verron. Four-vortex motion in the two layer approximation - integrable case. RXD, 2000.

[10] R. Gobato, A. Gobato, D. F. G. Fedrigo. Molecular electrostatic potential of the main monoterpenoids compounds found in oil Lemon Tahiti - (Citrus Latifolia Var Tahiti). Parana J. Sci. Educ. 2015, 1(1): 1-10. doi.org/10.5281/zenodo.3778400. URL: https://sites.google.com/site/pjsciencea/2015/november-v-1-n-1

[11] A. P. Crosta. Processamento digital de imagens de sensoriamento remoto. Campinas: IG/UNICAMP. 1992: 170.

[12] R. Gobato, M. Simões F. Alternative method of RGB channel spectroscopy using a CCD reader. Ciência e Natura, 2017, 39: 202-210. DOI: 10.5902/2179460X25617

[13] R. Gobato, A. Gobato, D. F. G. Fedrigo. Study of tornadoes that have reached the state of Parana. Parana J. Sci. Educ., 2 (1): 1-27, 2016. doi.org/10.5281/zenodo.3783851. URL: https://sites.google.com/site/pjsciencea/2016/january-v-2-n-1

[14] INPE. Available in: July 11, 2020. URL: http://satelite.cptec.inpe.br/acervo/meteosat.formulario.logic

[15] Navy Hydrography Center. Brazil's navy. Synoptic Letters. Available in: July 13, 2020. URL: https://www.marinha.mil.br/chm/dados-do-smm-cartas-sinoticas/cartas-sinoticas?field_data_value%5Bvalue%5D%5Bday%5D=1&field_data_value%5Bvalue%5D%5Bmonth%5D=6&field_data_value%5Bvalue%5D%5Byear%5D=2020&field_horario_value=12HMG

DOI: https://doi.org/10.30564/jasr.v3i3.2163

BILINGUAL PUBLISHING CO.
Pioneer of Global Academics Since 1984

Journal of Atmospheric Science Research
https://ojs.bilpublishing.com/index.php/jasr

ARTICLE

Development and Rapid Intensification of Tropical Cyclone OCKHI (2017) over the North Indian Ocean

Geetha B* **Balachandran S**

India Meteorological Department, Chennai, India

ARTICLE INFO

Article history
Received: 20 July 2020
Accepted: 28 July 2020
Published Online: 30 July 2020

Keywords:
Tropical cyclone
Ockhi
Asymmetry
Eddy flux convergence
Heat and moisture budget

ABSTRACT

Tropical Cyclone OCKHI over the North Indian Ocean during 2017 underwent dramatic development and rapid intensification very close to the land - Sri Lanka, extreme South Indian coast and Lakshadweep area during its initial developmental stage and caused extensive damages over these areas. On examining the physical and structural mechanism involved in such development, it is observed that the initial development was associated with axi-symmetrisation of the vortex that could be associated with Vortex Rossby waves near the eyewall. Associated with the expulsion of high vorticity from the centre during asymmetry mixing, there was outward propagation of eddy angular momentum flux in the lower levels that strengthened a low level anticyclone to the northeast of the TC centre which in turn enhanced the cyclonic inflow near the TC centre. The rapid intensification phase was associated with vertical non-uniform heating with upper and lower tropospheric warming associated with latent heat release in convection. During the mature phase, the system sustained 'very severe' intensity even under increasing vertical shear and lower ocean heat flux under the influence of a break in the sub tropical ridge to the north of the system centre that enhanced the poleward outflow in the upper troposphere.

1. Introduction

Tropical cyclone (TC) intensity changes occur through complex interaction of multi-scale physical and dynamical processes. Ocean heat fluxes, especially the latent heat flux (LHF) transfer at the sea-air interface, have long been recognized as important factors for the generation and maintenance of TCs [1]. Several studies have brought out the role of environment in TC intensity changes [2], DeMaria et al [3]). Rhome and Sethuraman [4] made a review of the processes identified to be associated with TC intensity change such as vertical wind shear (VWS), sea surface temperature (SST), upper level divergence, land interactions, eddy angular momentum fluxes etc. Some studies have also shown that even though environmental properties are important, they alone do not explain the intensity change problem. Hendricks et al. [5] found that the environments of rapid and slow intensification cases are similar and hence concluded that the rate of intensification may be only weakly dependent on environmental condition. Several studies have examined the role of storm-scale processes which are associated with the precipitation properties of TCs [6]. Bosart et al [7] have shown that TCs

**Corresponding Author:*
Geetha B,
India Meteorological Department, Chennai, India;
Email: geethab67@gmail.com

 DOI: https://doi.org/10.30564/jasr.v3i3.2177

undergo intensity changes under complex interaction between the large-scale environment, storm-scale processes and ocean-atmosphere coupling. Knaff et al. [8] found that the development of annular hurricanes was systematically preceded by a dramatic asymmetric mixing event between the eye and the eyewall involving one or more mesovortices. Montgomery and Enagonio [9] demonstrated the role of axi-symmetrisation mechanism in the development of a warm-core vortex and clarified the significance of axi-symmetrisation for tropical cyclogenesis. Corbaseiro et al [10] suggested that Vortex Rossby Waves (VRW) could result from expulsion of high vorticity from the eye during the asymmetry mixing and vorticity rearrangement in the vortex (axi-symmetrisation) and such VRWs could accelerate the tangential winds near the eye leading to inward shift of the radius of maximum wind and cause TC intensification. Such studies throw light on the TC processes and evolution. However, there are only limited studies on such processes for the TCs of the North Indian Ocean (NIO).

The very severe cyclonic storm (VSCS) OCKHI over the NIO during 29th November - 05th December 2017 underwent dramatic development and rapid intensification very close to Sri Lanka, Tamil Nadu-Kerala coasts (Comorin area) and Lakshadweep area during its initial developmental stage from 29th November/0300 UTC to 02nd December/0000 UTC and caused extensive damages over these areas. Subsequently, during its mature stage, it maintained VSCS intensity even under unfavourable environmental conditions. The Comorin area has been affected by only three cyclones in the past - during the period 1891-2016 and hence it is of scientific interest to understand the physical and structural mechanism involved in the development and intensification of TC OCKHI over the NIO during 29th November - 05th December 2017. Results of such studies, especially the present one regarding its initial development near the coast and rapid intensification during the formative stages, would help in improving our forecasting capabilities. Section 2 briefly describes the data and methodology used for analysis and Section 3 presents the results and discussions. Section 4 summarises the results.

2. Data and Methodology

The best track data from IMD, Ocean latent heat flux data fromWoodshole Oceanographic Institution [11], VWS product of Colorado State University - NOAA-NESDIS-CIRA based on AMSU, Low level convergence (LLConv), Upper level divergence (ULDiv) and Relative vorticity (RVor) from University of Wisconsin - CIMSS NCEP-FNL, 6-hrly, 1°x1° dataset are utilised for the present study. Using these datasets the environmental features, synoptic scale eddy interactions, dynamical parameter, convective structural asymmetries and thermo-dynamical features related VSCS OCKHI are analysed.

Synoptic scale eddy forcings have been shown to influence the intensification of TC MADI (2013) over the NIO [12]. For the present case, the role of synoptic scale eddy interactions is examined by computing Eddy angular momentum flux convergence (EFC) using NCEP-FNL, 6-hrly, 1°x1° dataset. The computation methodology adopted by Molinari and Vollaro [13] is used and is given by:

$$EFC = -\frac{1}{r^2}\frac{\partial}{\partial r} r^2 \overline{u'v'} \quad (1)$$

where u and v refer to storm relative radial and tangential velocities and prime refers to the deviations from the azimuthal mean; r is the radial distance from the TC centre. Computations are in storm relative cylindrical co-ordinate system up to 12˚ from the centre with radial interval Δr = 1°and azimuthal interval Δϕ = 15° using bilinear interpolation.

It has been shown that increase of diabatic heating with height near the TC centre in the mid-to-upper troposphere and increase of vertical inhomogeneous heating near the TC centre in the lower troposphere are favourable for RI and absence of upper tropospheric warming is a feature associated with rapid weakening (RW) [11,14]. The latent heat release associated with intense eyewall convection enhances the upper tropospheric warming of the core and lowers the central sea level pressure of the TC during the RI phase [15]. For examining this aspect in the present case, vertical profiles of apparent heat source and moisture sink are studied using NCEP-FNL 6-hrly, 1°x1° dataset based on the following heat and moisture budget equations [16]:

$$Q_1 = C_P\left[\frac{\partial T}{\partial t} + V.\nabla T + \left(\frac{p}{p_0}\right)^k \omega \frac{\partial \theta}{\partial p}\right] \quad Q_2 = -L\left[\frac{\partial q}{\partial t} + V.\nabla q + \omega \frac{\partial q}{\partial p}\right] \quad (2)$$

C_p is the specific heat capacity of air at const pressure, T: Temperature; V: Horizontal wind velocity, P: Pressure; ω: pressure vertical velocity, Θ: Potential temperature, k=R/C_p, L: Latent heat of condensation and q: mixing ratio of water vapour.

Under the influence of VWS and TC motion, it has been shown that there is a pronounced front-back asymmetry in TC convective structures [17]. It has also been shown that asymmetry maximum shifts cyclonically inwards during the intensification phase [12] and the asymmetry amplitude in the inner core is lower during RI events but, quite high during RW events [14]. As in these studies, asymmetry analysis for VSCS OCKHI is carried out based on Fourier first order wave number-1 asymmetry using TRMM based

DOI: https://doi.org/10.30564/jasr.v3i3.2177

0.25˚ x 0.25˚ rain rate data at 3-houly intervals (3B42v7) using the method followed by Lonfat et al. [18]. First, the mean rain rate in each 0.1˚ wide annulus (≈10 km) around the TC centre is computed up to 5˚ radial distance (50 annuli). For each annulus, the first order Fourier coefficients are computed using all individual rain rates as

$$a_1 = \sum_i [R_i \cos\theta_i]\ ,\ b_1 = \sum_i [R_i \sin\theta_i] \quad (3)$$

where R_i represents individual rain rates and θ_i, the phase angle of the corresponding grid point relative to the direction of motion of the TC. The spatial structure of the first order asymmetry can then be represented by

$$M_1 = \frac{\left[a_1 \cos\theta + b_1 \sin\theta\right]}{R} \quad (4)$$

where R is the mean rain rate calculated over the entire annulus. The asymmetry amplitudes are then normalised to the ambient mean rain rate of each annulus so that amplitude near unity implies that the wave number signal at that point is as strong as the axi-symmetric average.

3. Results and Discussions

Evolution of TC OCKHI under the influence of various oceanic and atmospheric environmental features and other large scale and storm scale dynamical processes are discussed below.

3.1 Synoptic History of VSCS OCKHI

The TC OCKHI formed as a low pressure area over southwest Bay of Bengal (BOB) and adjoining areas of south Sri Lanka on 28th November /0300 UTC and became well marked on 29th /0000 UTC over the same region. Under favourable environmental conditions, it concentrated into a Depression (D) over southwest BOB off southeast Sri Lanka coast on 29th / 0300 UTC. Moving westwards, it crossed Sri Lanka and emerged into Comorin area by 29th /1200 UTC. It intensified into a Deep Depression (DD) on 29th/2100 UTC. Moving northwestwards it intensified into a Cyclonic Storm (CS) on 30th / 0300 UTC over the Comorin area, into a Severe Cyclonic Storm (SCS) over Lakshadweep area on 01st December / 0000 UTC and further into a Very Severe Cyclonic Storm over southeast Arabian Sea (AS) to the west of Lakshadweep by 01st / 0900 UTC. Generally, for the NIO basin, TCs are considered to have undergone rapid intensification (RI)/ rapid weakening (RW) whenever there is 30 knots increase/decrease in maximum sustained surface wind speed (MWS; V_{max}) in 24 hrs [19]. In the present case OCKHI underwent RI during 01st/0000 UTC to 02nd 0000 UTC and attained its peak intensity of 150-160 kmph gusting to 180 kmph on 2nd /0900 UTC with lowest central pressure of 976 hPa over the AS. It then gradually recurved north-northeastwards, maintained its VSCS intensity till 04th / 1200 UTC and then weakened gradually. It crossed south Gujarat coast as a well marked low on 06th/0000 UTC. The system caused extensive damages over extreme south Tamil Nadu and south Kerala during its developmental stages on 29th-30th November. The system centre was about 60 km from Kanyakumari (Tamil Nadu), the southern most tip of peninsular India on 30th November / 0300 UTC when it intensified from DD to CS stage (as per IMD's best track data). Even though the system centre did not cross the coast and move inland, Kanyakumari and Thiruvananthapuram (Kerala) bore the brunt of the fury of the eye-wall region of the TC during 29th night-30th morning. The dynamical features and precipitation structures are analysed with regards to its initial developmental phase during 29th/0300 UTC to 30th/0300 UTC, rapid intensification phase during 01st/0000 UTC to 02nd 0000 UTC and its mature stage 03rd/1200 UTC to 04th/1200 UTC. The track of OCKHI as per the IMD's best track data is given in Figure 1.

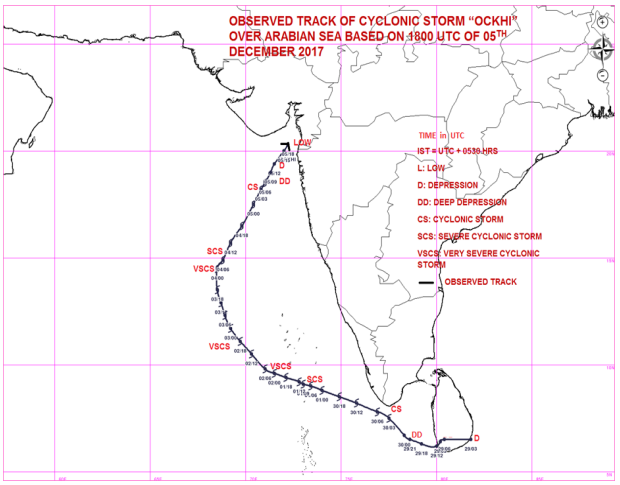

Figure 1. Track of TC OCKHI over the NIO during 29 Nov - 05 Dec 2017

3.2 Development and RI Phase

(1) Ocean-air latent heat flux and intensification of TC OCKHI

Figure 2a presents the time series of ocean-air LHF averaged over 6° lat/lon box centred at OCKHI's centre for 6-hrly positions and the MWS of TC OCKHI during the period 29th November - 05th December 2017. It is observed that LHF around the TC centre was >100 W/m^2 during its formative period (29th/0300 UTC to 30/0600 UTC) when its MWS increased from 25 kt to 40 kt. However, there was a steady decrease in the LHF in the vicinity of the TC centre (up to about 300 km from the

DOI: https://doi.org/10.30564/jasr.v3i3.2177

centre) from 135 W/m^2 to70 W/ m^2 during the period 30th/0600 UTC to 02nd December/0000 UTC when the MWS increased from 40 kt to 80 kt (pink box in Figure 2a). The TC also underwent RI during 01st/0000 UTC to 02nd/0000 UTC (yellow box in Figure 2a) even though, there was persistent decrease in the LHF around its centre. This suggests that the initial stages of development of the TC OCKHI was under the favourable influence of the LHF; however, the ocean-air LHF did not play any role in the system's further development and RI during the period 30th/0600 UTC to 02nd December/0000 UTC.

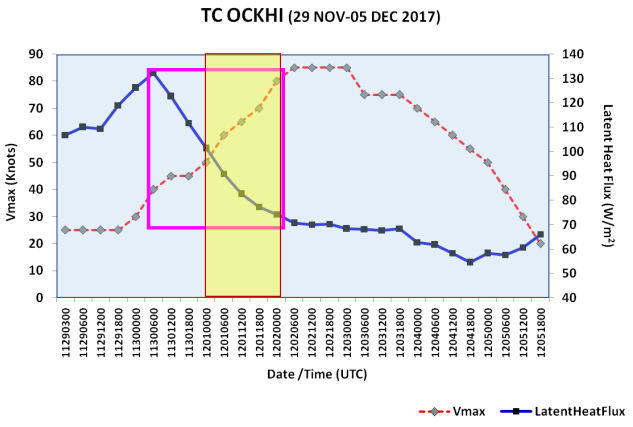

Figure 2a. Ocean-air latent heat flux (W/m2) and maximum sustained surface wind speed (Vmax in knots) during the life period of TC OCKHI over the NIO

(2) Vertical wind shear

Area averaged wind shear product for the 850-200 hPa layer as well as 850-500 hPa layer over 0-600 km from the TC centre taken from the real-time TC products of NOAA-NESDIS-CIRA is presented in Figure 2b. It is observed that during the initial period of formation from 29th November/1200 UTC to about 01st December/0000 UTC, there was a slight increase in the VWS around the TC centre from 10 kt to about 20 kt which decreased back to 10 kt during the RI phase (01st-02nd December / 0000 UTC). The system continued to be under low VWS of about 10 kt till 03rd / 0000 UTC after which, the VWS started to increase gradually. As such, the low VWS around the TC centre was favourable for its development and intensification.

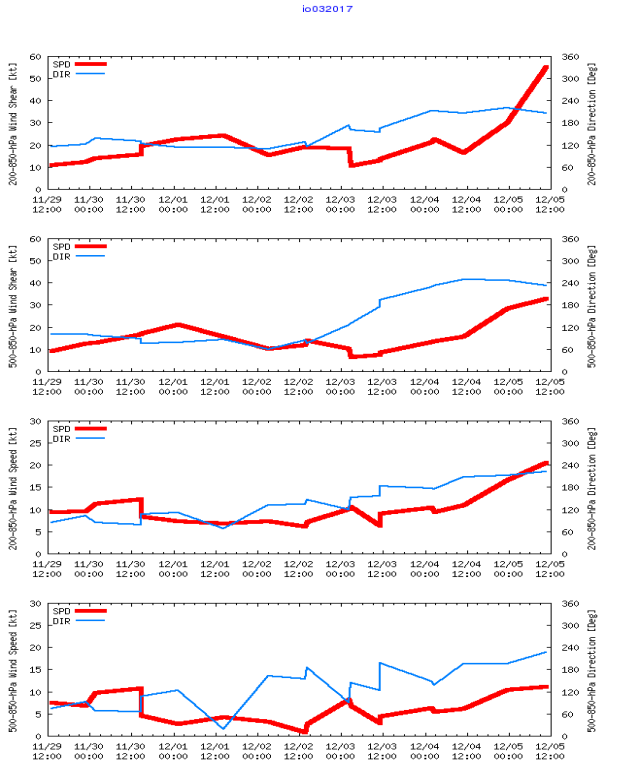

Figure 2b. Area averaged wind shear in the 850-200 hPa layer & 850-500 hPa layer over 0-600 km from the TC centre (Source: NOAA-NESDIS-CIRA TC products based on JTWC best track data)

(3) Synoptic scale eddy interaction

As detailed in Sec.2, the synoptic scale eddy forcings on the TC intensity changes is examined at the lower and the upper levels by computing the EFC at 850 hPa and 200 hPa levels up to about 1100 km from the TC centre. Figure 3a represents the EFC at 850 hPa during the initial development and RI phase of the TC OCKHI and Figure 3b, the radial velocity at 850 hPa during this period. It is observed that there was negative EFC in the inner core region (up to about 200 km from the TC centre) during the period 29th/1200 UTC to 29th/1800 UTC after which, there was outward propagation of EFC of 15-20 m/sec/day from about 300 km to 500 km during 30th/0000 UTC to 30th/1200 UTC. Even during the RI phase (01st/0000 UTC to 02nd/0000 UTC), there was some outward propagation of EFC (10-15 m/sec/day) at the outer radii (700 km -1000 km). The negative EFC during the initial stages indicates that there was no synoptic scale eddy forcing at the lower levels (i.e.) the system was not interacting with its environment during this period (29th/1200-1800 UTC). Such situations of the system not interacting with the environment can arise when the system's internal dynamics are very strong and do not allow the

DOI: https://doi.org/10.30564/jasr.v3i3.2177

environment to influence it. The enhanced low level convergence from 20 to 60 ($x10^{-5}$ s^{-1}), relative vorticity from about 150 to 250 ($x10^{-6}$ s^{-1}) at 850 hPa (Figure 3c&d) and enhancement of inward radial velocity from 29th/1800 UTC onwards (Figure 3b) are supportive of the indication that meso-scale processes at the inner core could be associated with the development of the system from the depression to CS stage.

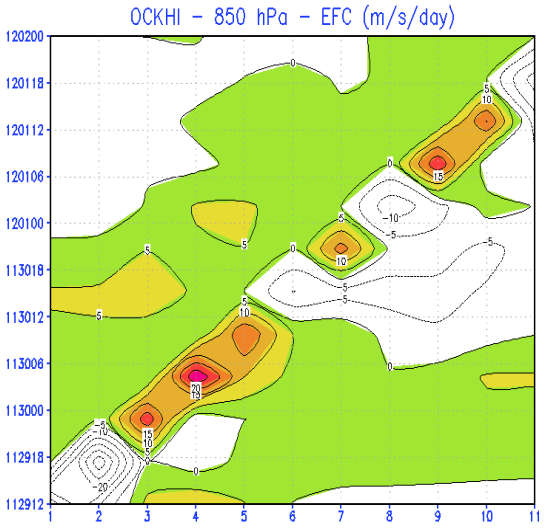

(a)

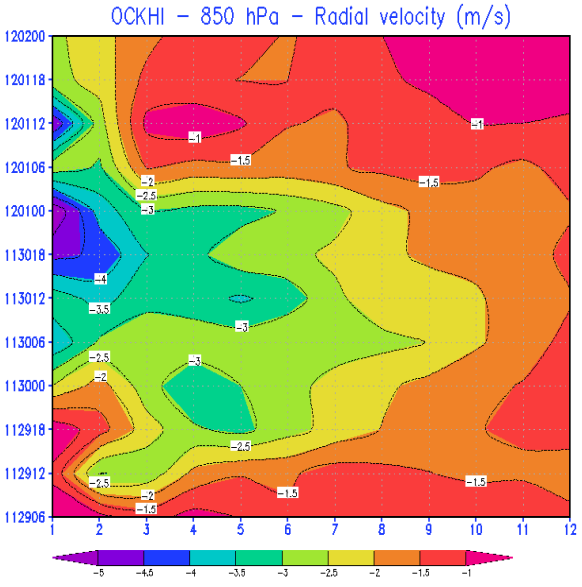

(b)

Figure 3a&b. 850 hPa Eddy Flux Convergence ($ms^{-1}day^{-1}$) (a) and Radial velocity (ms^{-1}) (b) from 100 km to 1100 km from the TC centre during the initial development and RI phase of TC OCKHI. x-axis represents the distance (in °lat/lon) from the TC centre and y-axis represents the date and time in mmddhh format

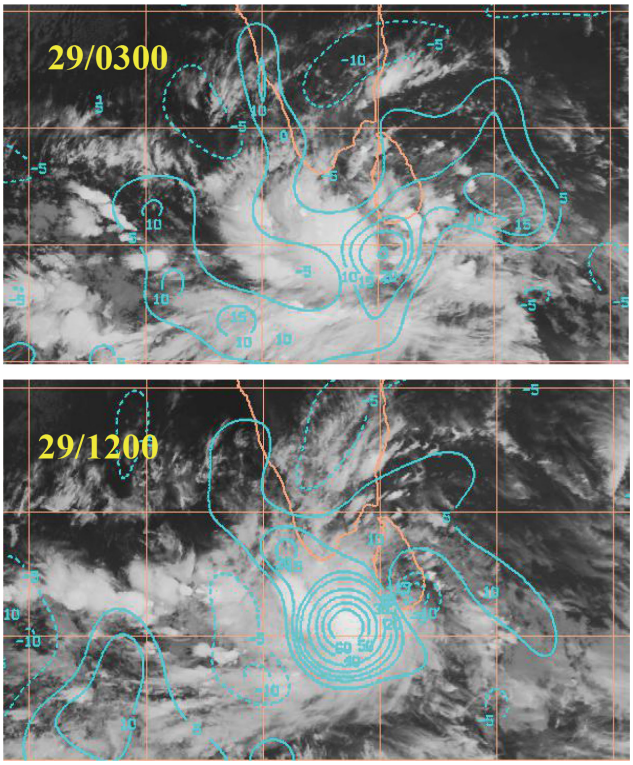

Figure 3c. NOAA-CIMSS product on low level convergence (x10-5 s-1) near the TC centre during 29th/0300 UTC and 29th/1200 UTC

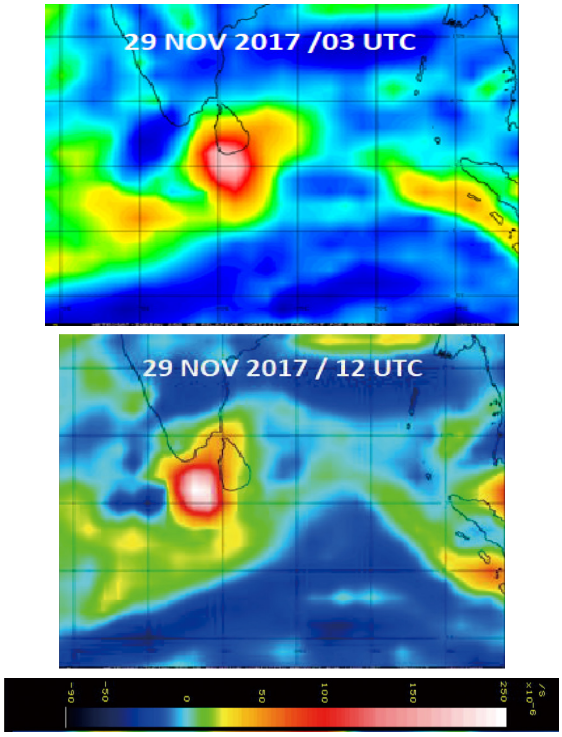

Figure 3d. NOAA-CIMSS product on relative vorticity ($x10^{-6}$ s^{-1}) near the TC centre during 29th/0300 UTC and 29th/1200 UTC

(4) Storm-scale processes

Several modelling and observational studies on meso-scale processes have examined the convective asymmetries in the context of axi-symmetrisation that leads to vortex intensification [20]. Interaction between asymmetries and their parent vortices has been advanced using potential vorticity (PV) dynamics and the recognition that PV (or Rossby type) waves exist in the vortex core.

Hence, the TC convective structure up to about 300 km from the centre is examined using Fourier first order wave number-1 asymmetry analysis as detailed in Sec.2. Figure 4a(1) presents the asymmetric structure associated with the TC during its development from depression to a CS. It is observed that large asymmetry is present in the inner core region (up to about 100 km from the centre) of the system on 29th/0600 UTC. Subsequently, by 29th/1200 UTC, the asymmetry maxima are pushed outwards and at 1800 UTC, it is pushed further outwards which is speculated as indication that asymmetry mixing leading to axi-symmetrisation of the vortex would have taken place in the inner core. By 30th/0600 UTC asymmetry maxima appear again in the inner core. However, symmetrisation of the vortex occurs again during the RI phase [Figure 4a(2), 01st December/1800 UTC].

The outward propagation of eddy angular momentum flux convergence (>10 m/sec/day which is taken as threshold for eddy interaction, DeMaria et al [3]) at 850 hPa level from 30th November/0000 UTC onwards (including the RI phase) from about 300 km from the TC centre up to about 1000 km from the centre could be envisaged as due to generation of VRWs . Such development of VRW could be verified through numerical experiments with very high resolution observational data in the vortex region.

Associated with the outward propagation of EFC, there was strengthening of a low level anti-cyclonic flow to the northeast of the system centre which in turn enhanced the cyclonic inflow into the system core (Figure 4b). This is supported by the sharp increase in inward radial velocity at 850 hPa from 3 m/sec to 5 m/sec near the inner core during 30th November, 1200 UTC to 01st December 0600 UTC (Figure 3b). The Windsat (37 GHz) microwave imagery depicting the low-mid level circulation as on 30th November / 0000 UTC shows a distinct centre (Figure 4c). Appearance of the nearly closed cyan + pink ring in the Windsat composite product is indicative of RI [21].

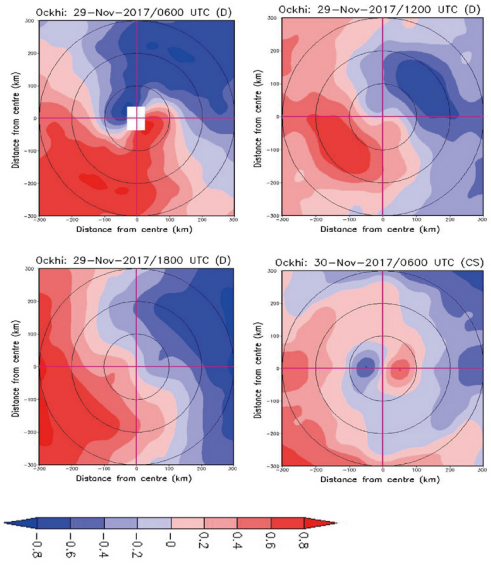

Figure 4a(1). Convective asymmetric structure up to about 300 km from the TC centre during the developmental phase of TC OCKHI - 29/0600 UTC, 1200 UTC, 1800 UTC and 30/0600 UTC, Nov 2017

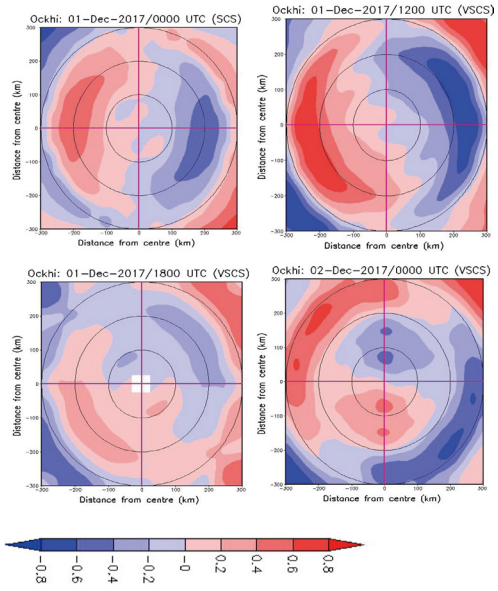

Figure 4a(2). Convective asymmetric structure up to about 300 km from the TC centre during the RI phase - 01/0000 UTC, 1200 UTC, 1800 UTC and 02/0000 UTC, Dec 2017

On examining the wind structure including the outer storm area using NOAA- NESDIS-MTCSWA data based on satellite retrievals at 6-hrly intervals during 30th November - 01st December, two azimuthal maxima (red) and minima (blue) are observed on 30th 0000 UTC and 0600 UTC in the outer storm area indicative of wave number 2 asymmetry (Figure 4d). However, this asymmetry decreases gradually during the RI phase and the system attains symmetric vortex by 01st December, 1200 UTC. In this connection, it may be mentioned that Reasor et al [22] and Corbosiero et al [10] have shown that

DOI: https://doi.org/10.30564/jasr.v3i3.2177

wave number 2 asymmetry in the spiral reflectivity bands outside the eye wall are associated with VRWs.

Figure 5 presents the longitude-vertical cross-section and latitude-vertical cross-section of heat and moisture at the end of the RI phase (01-02 December/ 0000 UTC). As noted in the earlier studies, a double maxima, one in the lower-mid troposphere and another in the mid-upper troposphere, is observed in Q1 and Q2 both in the longitude-vertical cross-section and latitude-vertical cross-sections. However, heating rate in the longitude-vertical plane is one order higher compared to that in the latitude-vertical plane. The heat source (positive Q1) and moisture sink (positive Q2) values are of the same order in both the cross-sections indicating that heating is mainly due to latent heat release due to convection. The Q1/ Q2 maxima located by about 400 km to the south/ north of the TC centre in the latitude-vertical cross-section could be associated diabatic heating in active spiral rainbands.

It is interesting to note that, in the latitude-vertical plane, there is a mid-tropospheric cooling (heat sink: negative Q1) and a moisture source (negative Q2) in the mid levels near the centre. In this regard, it may be mentioned that a study on thermodynamic pathway leading to RI of TCs in shear by Chen et al [23] indicates cooling in the 700-400 hPa layer mainly due to enhanced convective mixing associated with increase in convective bursts and the reduction of subsidence warming as the vortex aligns.

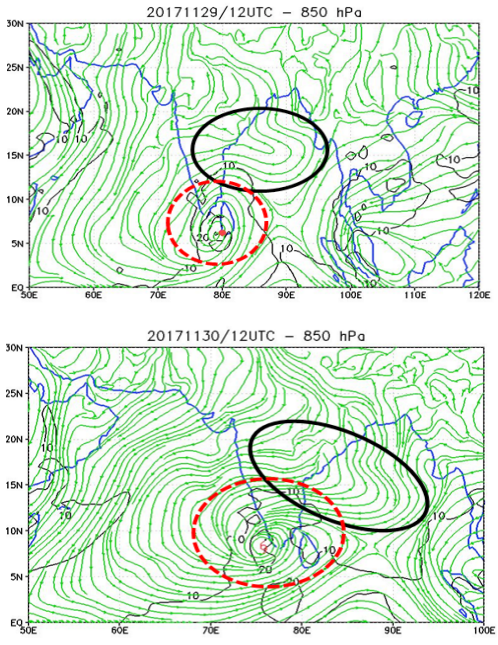

Figure 4b. 850 hPa streamline analysis for 29/1200 UTC and 30/1200 UTC, Nov 2017 (Location of TC centre is marked in red; Red dotted circle indicates the inflow region and black circle shows the anti-cyclonic circulation to the northeast of the system centre)

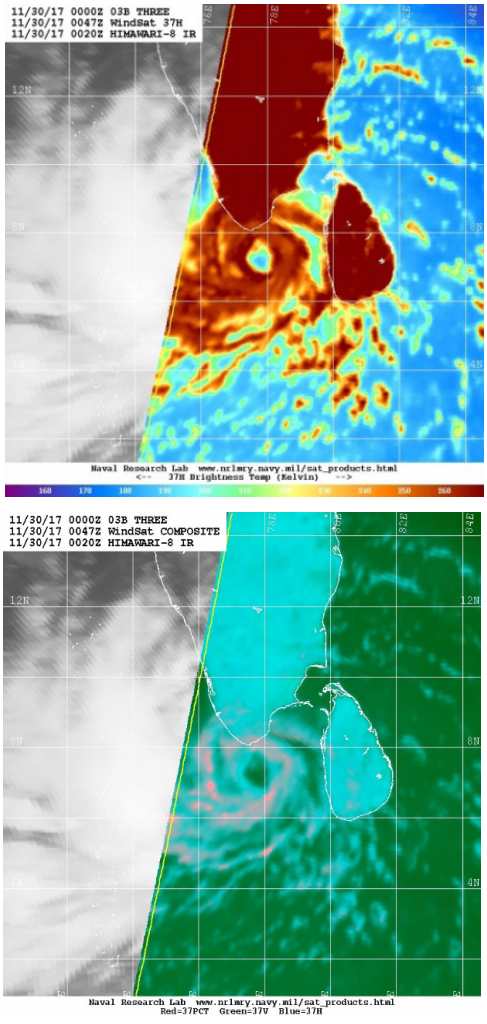

Figure 4c. Mirowave imagery of TC OCKHI as on 30 November, 00 UTC (Source: US-Naval Research Laboratory, Tropical cyclone page)

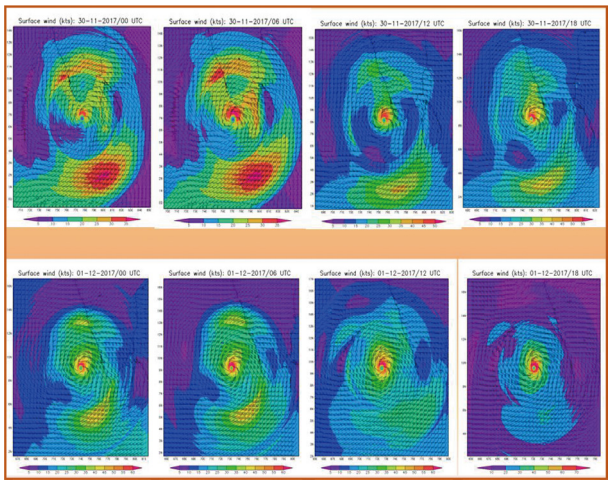

Figure 4d. Plots of satellite based NOAA-NESDIS-MTCSWA wind around the TC OCKHI at 6-hrly intervals on 30 Nov and 01 Dec 2017

 DOI: https://doi.org/10.30564/jasr.v3i3.2177

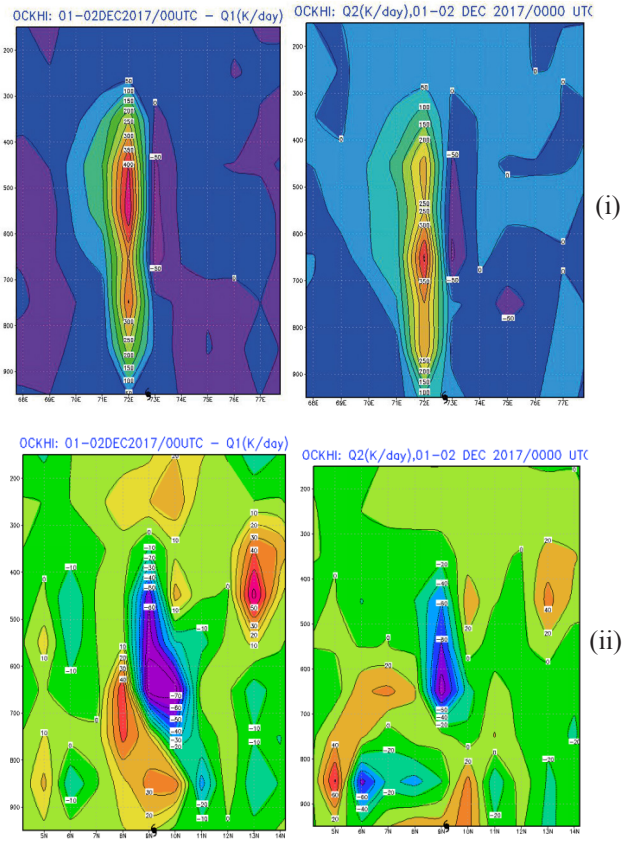

Figure 5. Vertical profiles of heat and moisture (K/day) in the (i) longitude- vertical cross-section (ii) and latitude-vertical cross-section during the RI phase of TC OCKHI

3.3 Mature Stage

During the period, 03rd December /1200 UTC to 04th/1200 UTC, the system maintained VSCS intensity even when the VWS was increasing and the ocean heat flux was less than 70 W/m^2 (Figure 1 & 2) under the influence of upper level eddy interactions. Figure 6(a&b) presents the 200 hPa eddy flux convergence and radial velocity during the life period of TC OCKHI. It is noted that until 03rd December / 0000 UTC there was no significant eddy interaction in the upper troposphere. Subsequently, EFC of the order of 10-20 m/sec/day is observed near the inner radii which expands outwards till 04th/1200 UTC (Figure 6a). Associated with this positive EFC, outward radial velocity at about 200-300 km from the TC centre increases from 4 m/sec to 12 m/sec during 03rd/0000 UTC to 04th/0000 UTC (Figure 6b). The eddy influence has been in the form of break in the sub tropical ridge and creation of enhanced outflow channel (Figure 6c) as observed in several earlier studies [24].

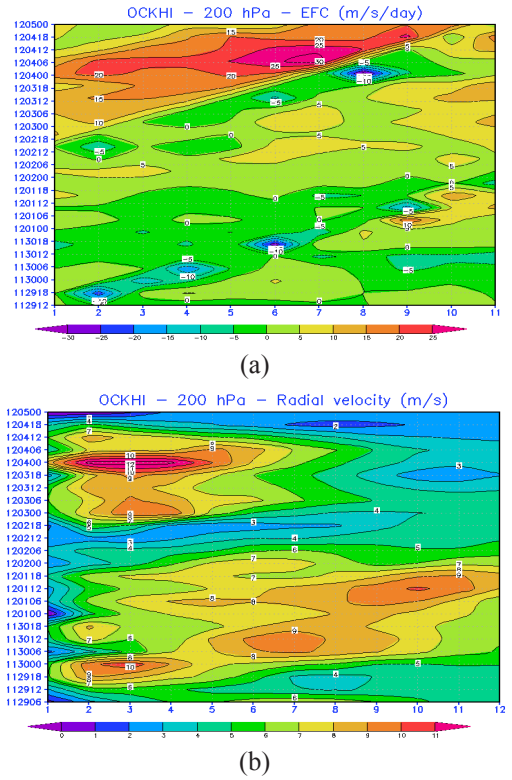

Figure 6a&b. 200 hPa eddy Flux Convergence (ms^{-1}day^{-1}) (a) and Radial velocity (ms^{-1}) (b) from 100 km to 1100 km from the TC centre during the life period of TC OCKHI. x-axis represents the distance (in °lat/lon) from the TC centre and y-axis represents the date and time in mmddhh format

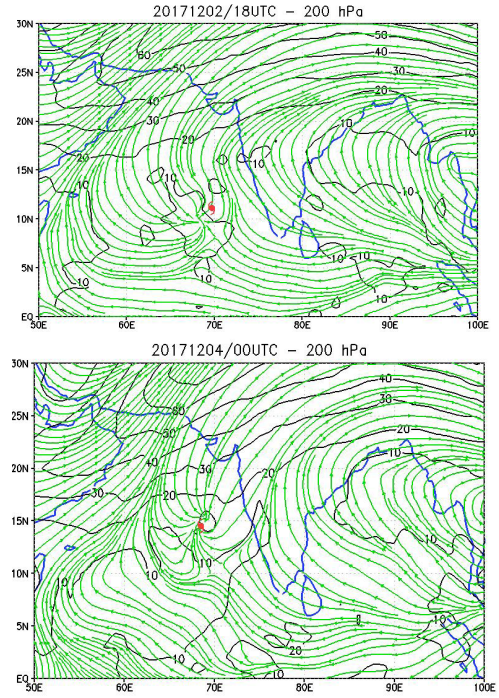

Figure 6c. 200 hPa streamline analysis as on 02nd/1800 UTC and 04th/0000 UTC, Dec 2017 (Location of TC centre is marked in red)

DOI: https://doi.org/10.30564/jasr.v3i3.2177

4. Summary

The physical mechanisms and structural changes involved in the development and intensification of TC OCKHI over the NIO during 29th November - 05th December 2017 is studied. OCKHI underwent dramatic development and rapid intensification during the period 29th November/0300 UTC to 02nd December/0000 UTC even as the ocean heat fluxes near the TC centre decreased sharply. However, the system was in a low-moderate VWS environment and the initial development of OCKHI was associated with axi-symmetrisation of the vortex as observed in the wave number-1 asymmetry in the convective structure which could be associated with Vortex Rossby waves near the eyewall.

Wave number-2 asymmetry in the outer storm area which has been identified with VRWs in some other works is seen in the wind structure during this period. Associated with the expulsion of high vorticity from the centre during asymmetry mixing and vorticity rearrangement, there was outward propagation of eddy angular momentum flux in the lower levels. This strengthened a low level anticyclone to the northeast of the TC centre which in turn enhanced the cyclonic inflow near the TC centre. During the RI phase, there is upper and lower tropospheric warming associated with latent heat release in convection. A mid level cooling is also observed during RI which could be due to enhanced convective mixing associated with increased convective bursts during asymmetry mixing and vorticity expulsion. During the mature phase of the TC, the system sustained VSCS intensity even under increasing VWS and lower ocean heat flux under the influence of a synoptic scale eddy forcing in the upper troposphere in the form a break in the sub tropical ridge to the north of the system centre which enhanced the poleward outflow channel and maintained the system. Further studies with numerical simulation with high resolution observational data from RADAR and satellite are required to substantiate the above results.

Acknowledgments

The authors thank the Director General of Meteorology, India Meteorological Department for providing facilities to undertake this study. Use of NCEP reanalysis and FNL data, TRMM rainfall data, NOAA-CIMSS satellite based tropical cyclone products, NOAA-NESDIS MTCSWA data, Woodshole Ocenographic Institution's OAFLUX data and US-NRL microwave products are duly acknowledged.

Conflicts of Interest

The authors declare no conflict of interest.

References

[1] Riehl, H. Tropical Meteorology[M]. McGraw-Hill, 1954.

[2] Merrill, R.T. Environmental-influences on hurricane intensification[J]. J. Atmos. Sci, 1988, 45: 1678-1687.

[3] DeMaria, M., Baik, J.J., Kaplan, J. Upper-Level Eddy Angular Momentum Fluxes and Tropical Cyclone Intensity Change[J]. J. Atmos. Sci., 1993, 50(8): 1133-1147.

[4] Rhome, J.R., Sethuraman. Environmental influences on tropical cyclone structure and intensity: a review of past and present literature[J]. In. J. Mar. Sci., 2006, 35(2): 61-74.

[5] Hendricks, E.A., Peng, M.S., Fu, B., Li, T. Quantifying Environmental Control on Tropical Cyclone Intensity Change[J]. Mon. Wea. Rev., 2010, 138: 3243-3271.

[6] Stevenson, S. N., Corbosiero, K.L., Molinari, J. The convective evolution and rapid intensification of Hurricane Earl (2010)[J]. Mon. Wea. Rev., 2014, 142: 4364-4380,
DOI: 10.1175/ MWR-D-14-00078.1

[7] Bosart, L. F., Velden, C.S, Bracken, W.E., Molinari, J., Black, P.G. Environmental influences on the rapid intensification of Hurricane Opal (1995) over the Gulf of Mexico[J]. Mon. Wea. Rev., 2000, 128: 322-352.

[8] Knaff, J.A., Kossin, J.P., DeMaria, M. Annular hurricanes[J]. Wea. Forecasting, 2003, 18: 204-223.

[9] Montgomery, M.T., Enagonio, J. Tropical cyclogenesis via convectively forced vortex rossby waves in a three-dimensional quasi-geostrophic model[J]. J. Atmos. Sci, 1998, 55: 3176-3207.

[10] Corbosiero, K.L., Molinari, J.; Aiyyer, A.R., Black, M.L. The structure and evolution of hurricane Elena (1985) Part II: Convective asymmetries and evidence of Vortex Rossby Waves[J]. Mon. Wea. Rev. 2006, 3073-3091.

[11] Yu, Yubin., Xiuping, Yao. Thermodynamic Characteristics of Tropical Cyclones with Rapid Intensity Change over the Coastal Waters of China[J]. Acta Meteorologica Sinica, 2010, 25(4): 467-477.

[12] Balachandran, S., Geetha, B. Diagnostics of Upper Level Dynamics and Rainfall Asymmetry of Very Severe Cyclonic Storm MADI (2013)[M]. In Tropical Cyclone Activity over the North Indian Ocean (Eds. Mohapatra et al), Capital Pub Co., New Delhi, 2016.

[13] Molinari, J., Vollaro, D. External Influences on Hur-

 DOI: https://doi.org/10.30564/jasr.v3i3.2177

ricane Intensity, Part I: Outflow Layer Eddy Angular Momentum Fluxes[J]. J. Atmos. Sci., 1989, 46(8): 1093-1105.

[14] Geetha, B., Balachandran, S. Diabatic heating and convective asymmetries during rapid intensity changes of tropical cyclones over North Indian Ocean[J]. Tropical Cyclone Research & Review, 2016, 5(1-2): 32-46.

[15] Wang, H., Wang, Y. A numerical study of Typhoon Megi (2010). Part-I: Rapid Intensification[J]. Mon. Wea. Rev., 2014, 142: 29-48.

[16] Yanai, M., Esbensen, S., Chu, J.H. Determination of bulk properties of tropical cloud clusters from large scale heat and moisture budgets[J]. J.Atmos. Sci., 1973, 30: 611-627.

[17] Chen, S.S., Knaff, J.A., Marks Jr, F.D. Effects of vertical wind shear and storm motion on tropical cyclone rainfall asymmetries deduced form TRMM[J]. Mon. Wea. Rev., 2006, 134: 3190-3208.

[18] Lonfat, M. Marks J,. F.D., Chen, S.S. Precipitation Distribution in Tropical Cyclones Using the Tropical Rainfall Measuring Mission (TRMM) microwave imager: A global perspective[J]. Mon. Wea. Rev., 2004, 132: 1645-1660.

[19] Kotal, S.D., Bhowmik, S.K.R. Large scale Characteristics of rapidly intensifying Tropical Cyclones over the Bay of Bengal and rapid intensification Index[J]. Mausam, 2013, 64(1): 13-24.

[20] Montgomery, M.T., Kallenbach, R.J. A theory for vortex Rossby-waves and its application to spiral bands and intensity changes in hurricanes[J]. Quart. J. Roy. Meteor. Soc., 1997, 123: 435-465.

[21] Kieper, M., Jiang, H. Predicting tropical cyclone rapid intensification using the 37 GHz ring pattern identified from passive microwave measurements[J]. Geophys. Res. Lett., 2012, 39: L13804. DOI: 10.1029/2012GL052115

[22] Reasor, P.D., Montgomery, M.T., Marks Jr, F.D., Gamache, J.F. Low wavenumber structure and evolution of the hurricane inner core observed by airborne dual-Doppler radar [J]. Mon. Wea. Rev., 2000, 128: 1653-1680.

[23] Chen, X., Zhang, J. A., Marks, F.D. A thermodynamic pathway leading to rapid intensification of tropical cyclones in shear[J]. Geophys. Res. Lett, 2019, 46: 9241-9251.

[24] Rucker, J.H. Upper-Tropospheric Forcing on the Intensification Rates of Tropical Cyclones Flo and Ed based on TCM-90 observations[D]. Masters' Thesis - Naval Postgraduate School, Monterey, California, 1992.

DOI: https://doi.org/10.30564/jasr.v3i3.2177

BILINGUAL PUBLISHING CO.
Pioneer of Global Academics Since 1984

Journal of Atmospheric Science Research
https://ojs.bilpublishing.com/index.php/jasr

ARTICLE

Influence of the 60 Hz Magnetic Field on the Airborne Microbial Distribution of Indoor Environments

Matilde Anaya[1] Sofia F. Borrego[2*] Miguel Castro[3] Oderlaise Valdés[2] Alian Molina[2]

1. Food Industry Business Group (GEIA), Avenida del Puerto s/n entre Hacendado y Atarés, Havana, Cuba
2. Preventive Conservation Laboratory, National Archive of the Republic of Cuba (ARNAC). Compostela 906 esq San Isidro, Havana, Cuba
3. Electric Researches and Tests Center, Faculty of Electric Engineering, Polytechnic University "José A. Echeverría" (CUJAE), Havana, Cuba

ARTICLE INFO

Article history
Received: 22 July 2020
Accepted: 28 July 2020
Published Online: 30 July 2020

Keywords:
Non-ionizing radiation
Appliances
Airborne mycobiota
Indoor environment
Index of microbial air
Magnetic field

ABSTRACT

The aim of this work was to analyze the effect of the magnetic field generated by the household appliances on the airborne microbial surrounding these equipment located on indoor environments with particular interest in the environmental fungi. A simultaneous environmental study was carried out in locals of three different geographical places of Havana, Cuba, which have televisions, computers and an electric generator. The air samples were made by a sedimentation method using Malt Extract Agar. The concentration of total aerobic mesophilic as well as fungi and yeasts were determined in rainy and little rainy seasons by applying as factors: exposure time of dishes (5 to 60 min) and distance to the wall (0 and 1 m) at a height of 1 m above the floor. The predominant fungal genera were *Cladosporium, Penicillium and Aspergillus*. In the dishes that were placed at 0 and 0.5 m from the emitting sources were observed that some bacteria colonies formed inhibition halos, a great diversity of filamentous fungi and an increase in the mycelium pigmentation as well as the pigments excretion. In the rainy season, the highest amounts of fungi were obtained in all samples. In the little rain season the count of the Gram-negative bacilli increased three times the Gram-positive cocci.

1. Introduction

It is well-known that fungi and their propagules (spores and cellular fragments) are an important source of allergens. Its distribution is ubiquitous, universal and they behaving as allergens which contribute to triggering numerous diseases [1]. When the symptoms are described for the indoor occupants, caused by microorganisms and other contaminants, are referred to Sick Building Syndrome (SBS) [2]. Therefore, microbiological contamination of indoor air is of great importance because many people perform up to 90% of their activities in these spaces. The microbial contamination of the air of these places, mainly by fungi (aeromycobiota), is considered one of the greatest threats to health, since it can be ten times greater than the outdoor [3], although another author states that it is from six to seven times smaller [4].

The impact of the electric generators (EG) on the

**Corresponding Author:*
Sofia F. Borrego,
Preventive Conservation Laboratory, National Archive of the Republic of Cuba (ARNAC). Compostela 906 esq San Isidro, Havana, Cuba;
Email: sofy.borrego@gmail.com; sofy.borrego@rediffmail.com

 DOI: https://doi.org/10.30564/jasr.v3i3.2215

environment at different stages of their life cycle [5] and its location requires study which takes into account risks to the health of the population and the workers, in both phases construction and operation [6]. In this sense, most cases of EG studies are limited to the generation of electric and magnetic fields [7,8], noise emissions and physical-chemical air [9,10] but the microbiological quality of air is not studied and it is very important for human activity [11-15].

It is known that different physical factors influence in the dynamics of the behavior of biological aerosols [4]. It is known that different physical factors influence in the dynamics of the behavior of biological aerosols. Its characterization depends on the method of sampling and the analysis used but currently a standard protocol to evaluate the contamination and their effect in indoor environments is not available. Therefore, it is difficult to compare the results of a study with other one carried in the same country or in other geographical areas [3]. According to Gent (2003) [16] count can be classified into four levels: no detectable (0 CFU/m^3), low (1 to 499 CFU/m^3), means (500 to 999 CFU/m^3) and high (1000 or more CFU/m^3). In response to this classification, the private homes are considered with a mean value of contamination (600 - 800 CFU/m^3) whilst the dressing rooms have a high contamination (800 - 1500 CFU/m^3). In general, at indoors environments are acceptable between 100 to 500 CFU/m^3 but only it is accepted 50 CFU/m^3 if are pathogenic fungi such as *Aspergillus* spp.

Moreover recent researches show that environmental fungi were stimulated by nuclear radiation that persist in the surrounding areas to the power plant Chernobyl [17-19] and the environmental study made in a local closed showed that a similar phenomenon occurred with magnetic field density (B) of 10 mT and 60 Hz for 220 V [20]. In this investigation the fungal propagules were attracted and deposited on the Petri plates located near the magnetic field generator coil in the same way that occurred with the bacteria under a 4 kV electric field [21]. There is a great diversity of B in the environment of different electrical equipment, even of similar characteristics, whose value does not depend on its size, complexity, power or the noise that can make each domestic appliance [22]. In addition, it should be highlight that the extremely low frequencies the electric field is obstructed by any obstacle while the magnetic field only decreases as it moves away from the source.

It is proposed that electromagnetic waves can influence the distribution of the aeromicobiota in indoor environments. The trajectory of the spores of the fungus *Drechsrela turcica* was studied and it was shown that they have electric charge since they were attracted to the electrode through which circulated alternating current of 115 V/50 Hz [23]. More recent studies apply this property of fungal spores but under the action of an electrostatic field between 0.5 and 5 kV [24-26]. According to Jamieson and Jamieson (2006) [21] the electrical and magnetic fields generated by the equipment can attract pathogenic bacteria inside the locals like offices and hospitals increasing the risk of contamination by this way. For this reason the aim of this work was to analyze the effect of the magnetic field generated by electrical household appliances on the aeromicobiota surrounding these equipment located in indoor locals.

2. Materials and Methods

The environmental studies of interiors were carried out in three geographical areas of Havana, Cuba (Table 1). The premises studied are located in there municipalities Lisa, Arroyo Naranjo and East of Havana (at West, South and East of city, respectively). Two different days corresponding to the rainy and little rainy seasons of the years 2017 to 2018 were simultaneously sampled (Table 2).

Table 1. Description of the equipment used in this research according to the geographic location of the premises in the city

Equipment	Brand/ Country	Dimentions of the locals (m)	Neighborhood/ Municipality	Geographic location of the premises in the city
Personal Computer (PC)	AOpen/ Taiwan	3 x 2 x 2.2	Guatao/Lisa (LI)	West
Electric Generator (EG)	Genesal/ Spain	6 x 4 x 3.0		
Television (TV)	Atec Panda/ Korea	7 x 3 x 2.5	Alamar/ East of Havana (EH)	East
	LG/Korea	3 x 3 x 2.5	Electric/ Arroyo Naranjo (AN)	South

Note: *these acronyms were used to identify the equipments and their locations.*

Table 2. Thermo hygrometric values of outdoor environment each day studied according to report of weather station located in Havana city

Seasons	Day of microbiological indoor air sampling	Outdoor Temperature (ºC)			Outdoor Relative Humidity (%)
		medium	max	min	
Rainy	14th May 2017	26.6	31.4	23.2	75
	1st June 2017	24.9	30.2	22.8	89
Little rainy	27th December 2017	23.4	30.8	19.9	82
	4th January 2018	24.7	29.0	20.8	84

DOI: https://doi.org/10.30564/jasr.v3i3.2215

Note:

Report of Weather Station 783250 "White House" (latitude: 23.16; longitude: -82.35; altitude: 50) of the Cuban Institute of Meteorology (http://www.tutiempo.net/clima/CASA_BLANCA/783250.htm).

The EG (Genesal, Spain, Power 47/51 kVA) was selected because it is located 6 m from away to the PC-LI in Guatao. TVs and computers were selected because they are the household appliances most used in the home and people stay in front of them for several hours and with similar daily frequencies for both [22].

The variables temperature and relative humidity of the locals were taken with a digital thermo hygrometer (Hygro-thermometer DHT-1, China) which scales of temperature is from 5 to 50°C and 0.1°C with accuracy and relative humidity from 10 to 100% with accuracy 1%. The measurements of density of the magnetic field were taken with a gaussmeter (Enertech, EmdexII, USA) of scale 1 to 3000 and 0.1 mG of precision.

As in most homes there are TVs, with the results obtained in the sampling of the premises with this appliance, a D-optimal multifactorial design was applied by the statistical program Design Expert version 6.0.1.0 (STAT Ease, Minneapolis). The experimental factors studied were: the exposures time of the Petri dishes, the distance from the PCs to the wall as well as the geographical location of the room where the TVs are located (Table 3). A total of 17 experimental runs were obtained and total aerobic mesophilic (TAM), fungi and yeasts (FY) were determined.

Table 3. Levels of the factors studied in the experimental design

Level	Factors		
	Exposure time (min)	Distance of the TV (m)	Localization of the TVs
1	5 (low)	0 (low)	Arroyo Naranjo (TV-AN)
2	60 (high)	1 (high)	East of Havana (TV-EH)

When exposing of the Petri dishes with Plate Count Agar and Malt Extract Agar to determinate TAM and FY, respectively it was taken into account that the household appliances are usually placed 5 to 10 cm from the wall. This distance was assumed as 0 m and from this was added up to 1 m in correspondence with the experimental design (Table 3) and according to Pasquarella et al. (2000) [4]. In this way the same conditions in the three locations were guaranteed. For the sampling, a diagonal design with 3 or 5 points was followed (Figure 1).

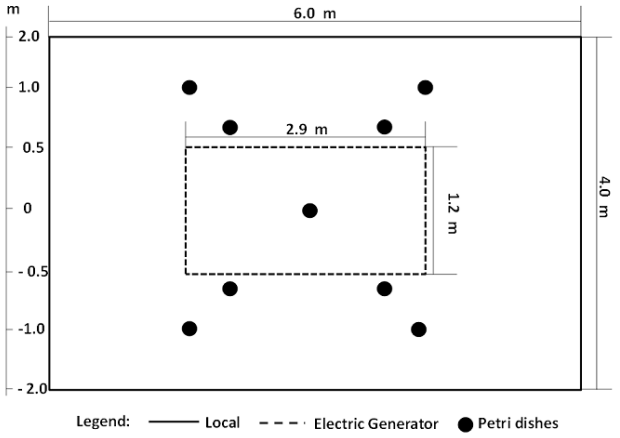

Figure 1. Representative scheme of the location of Petri dishes during the microbiological sampling of the air in a local (6 x 4 x 3 m) with an electric generator (EG) (2.9 x 1.2 x 1.3 m). The center of the generator was taken as distance 0 m, the Petri dishes were placed at five diagonal points and the microbiological environmental index was applied (1 m from the walls: 1 m from the floor: 1 h of opened Petri dishes)

After the incubation of Petri dishes at 30ºC for 5 days, the count was done to determine the microbial concentration expressed in Colony Forming Units per m^3 of air (CFU/m^3) according to the equation described by Omeliansky [27-29]:

$N = 5\ a.10^4\ (bt)^{-1}$

Where N: microbial concentration (CFU/m^3), a: number of colonies per Petri dish, b: dish surface (cm^2), exposure time (min).

With the values obtained the distribution a map of microbiological contamination in said premises using the Surfer v.8 software was built, according to a similar study [12].

Cultural and morphological characteristics of fungal colonies as well as conidiophores and conidia fungal structures were observed (stereomicroscope at 14X and trinocular Olympus microscope brand Samsung with digital camera coupled SCC-101 AP, 40X) and the identification was performed according to different manuals [30-33]. Bacteria were typified according to the morphology and Gram stain.

Analysis of relative frequency (RF) of occurrence of the detected fungal genera in the premises was expressed in percentage, using the following equation:

RF = Times a genus is detected/Total number of sampling realized x 100

At each point the sampling were performed in triplicate and the appliances turned off were took as control samplings. The data was analyzed with the program

 DOI: https://doi.org/10.30564/jasr.v3i3.2215

Statgraphics Centurion XV.

3. Results and Discussion

In the colony count a concentration between 38 and 1060 CFU/m^3 of air was obtained for temperature and relative humidity average values of 27 ± 2°C and 82 ± 5%, respectively. Therefore, microbiological contamination of the premises can be classified with low to medium with counts of filamentous fungi (into the FY group) similar to the result informed for environmental indoors in Havana previously [15]. There were statistically significant differences ($p \leq 0.05$) between concentrations of TAM and FY but also between different levels of the factors studied.

For 5 minutes of exposure of the Petri dishes less variability of the colonies was obtained with respect to 1 h, which shows that the sensitivity of the technique can be increased by increasing the time of exposure, like was demonstrated in other similar research previously [20]. This is important for allergists, since a great deal of information can be obtained about prevailing fungi that may even contaminate food [34,35].

Figure 2 shows the average values of the microbial concentration in the Petri dishes exposed for 1 h at the three locations.

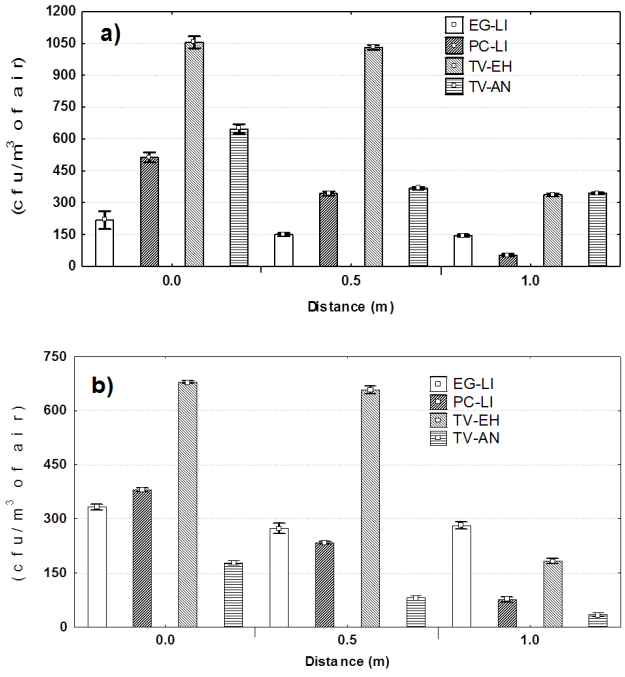

Figure 2. Microbial concentration (CFU/m^3 air) in three locals where the Petri dishes were exposed for 1 hour, 1 m above ground level and 1 m separated from walls in the rainy season of 2012. a) total aerobic mesophilic, b) fungi and yeasts

According to various studies, fungi count can vary within a large range depending on the methodology used and other determinants as the geographic area where the study was focused [1]. Since in all research the same methodology was used, statistically significant difference found in microbial concentrations obtained around appliances can be given by their geographic location. In that sense, the concentrations obtained at the same premises located in Lisa showed significant difference between the equipment groups (EG and PC), whilst there was significant difference between these premises and the others located in EH and AN consistent with those reported in an environmental study previously conducted in different locations in Havana [3].

At the distance of 0 m, all the studied premises had high pollutions, being the highest microbial concentration for TV-EH, followed in descending order: TV-AN, PC-LI and EG-LI. It should be noted that these values could be influenced by the sedimented dust on the equipment, since it has been suggested that microbial air pollution influences the microbial contamination of surfaces [13]. The particular behavior of the fungal concentration in front of TVs and EG-LI was studied in detail later.

By analyzing of the distance to the appliances (longer distance, lower density of OMF), similarity between the values to 0 and 0.5 m was observed, which they were higher than 1 m (Figure 2). This behavior was similar to those observed in other studies which showed that the bacteria were attracted up to the Petri dishes placed at 1 m distance to electric field of 4 kV [21] and the fungi to the Petri dishes located in front of the electric transformers which were emitting 0.4 to 1.2 mT [36]. Although in this investigation the observed behavior was similar for all appliances it is evident that the low values of OMF generated by these equipment cause the same effect and can be related to the increase of the electrostatic charge that concentrate the positive ions [37].

The settled dust is an important factor to be taken into account because this can have many species of fungi and yeasts xerophilic that commonly not float in the air [3]. In this sense, it is known that the genus *Cladosporium* is found in both indoor and outdoor environments and its presence in the dust could be due to fragments of spores that sediment [38] and they are present together with spores of the genus *Cephalosporium* and *Penicillium* even after cleaning with a vacuum cleaner [39]. However, considering the possible influence of the sedimented dust on the environmental microbial concentration, a contradiction is evident with the values obtained close to the EG-LI since a low microbial concentration was detected that contrasts with the large size and surface of this equipment (where a large amount of sedimented powder should be

DOI: https://doi.org/10.30564/jasr.v3i3.2215

accumulated) with respect to the remaining equipments as well as the possible value of OMF it generates (0.1 and 0.6 μT for PCs, 0.8 and 23.5 μT for TVs and 0, 01 and 0.5 mT, for EG). This result can be explained taking into account the dispersion of the dust particles generated by the combustion gases during the EG operation, which makes it possible to suppose that these gases contributed to the decrease of the aeromicrobiota of the place where the EG is located.

Figures 3 and 4 present examples of growth in Petri dishes exposed for 1 h in different positions at the three locations. At a shorter distance the obtained bacterial colonies formed inhibition halos (Figures 3 c, 4 j, 4 o and 4 s) and a greater variety of filamentous fungi were observed whose colonies showed more pigmentation (Figures 4 c, f, g, h, m, and p). This variation in the colonies pigmentation was more significant for those isolated from the surroundings of the televisions and personal computers.

However, at 0 m distance the increase in the mycelial growth size and the pigmentation of the colonies could be influenced by the effect of the magnetic field, since in all the dishes close to the equipment the colonies pigmentation was observed: (orange color in Figures 4 b, c, h, and m) and coloring of the culture medium (fuchsia color in Figures 4 c, f, g, h, p, and q). In this regard, with 25 mT obtained from 50 Hz, stimulating effects were found in several fungi strains when were exposed for 4 h to 10 days [40,41]. It is suggested that this phenomenon of increased pigmentation occurs in fungi and other microorganisms to protect against the lethal effect of electromagnetic radiation [42]. This behavior is significant since it is an indicator of cellular metabolism (excretion of toxins and other metabolites that are allergenic and toxic), which shows that these fungal genera are present in similar environments including the environments where the electrical appliances studied are located.

Because pigmentation in fungal colonies is an adaptive response to the effect of such radiation [42] these strains of fungal species could be used in laboratory studies to evaluate the effects of higher values of B at 60 Hz frequency. Consistent with the above, to these distances from the EG-LI different fungal species was observed which excreted pigments and stained the culture medium. It should highlight that the dematiaceous and hyaline fungi that excrete pigments into the culture medium were detected more frequently at the 0 and 0.5 m distances of the EG-LI whilst at a distance of 1 m (lower magnetic field density or B) only were detected the hyaline fungi that do not excrete pigments (Figures 4 p and 4 q). Both the mycelium pigmentation and the pigments excretion to outside and therefore the staining of the culture medium are indicative of the fungal metabolic activity.

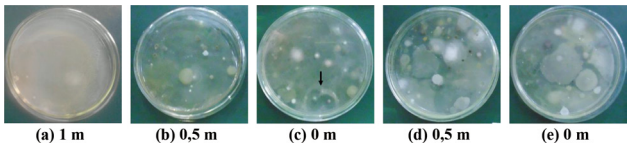

Figure 3. Colonies of total aerobic mesophilic (TAM) at different distances from a personal computers located in Guatao, Lisa (a, b and c) and a television located in Alamar, East of Havana (d and e) in the rainy season. The arrow indicates the formation of inhibition halos

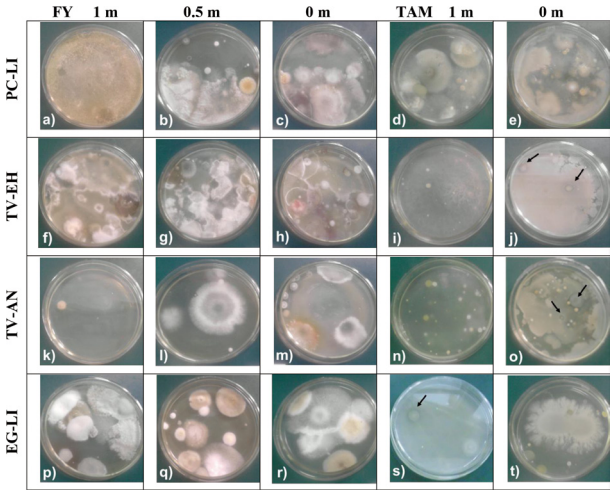

Figure 4. Microbial colonies obtained at different distances from personal computers and an electric generator located in a local of Guatao, Lisa (PC-LI and EG-LI), televisions located in homes of Alamar, East of Havana (TV-EH) and the neighborhood "Electric", Arroyo Naranjo (TV-AN) during the rainy season. FY: Fungi and Yeasts; TAM: Total Aerobic Mesophilic. The arrow indicates the formation of halo of inhibition

As in both studies this phenomenon occurred with a value of B in the order of the microtesla (μT) it is inferred that the value of B at 60 Hz must be in the order of militesla (mT) [20] to observe an effect of attraction or reorientation of the aeromicrobiota of indoor environments towards the sources of emission of the magnetic field. That is, for an electric current of 60 Hz the very low values of B are sufficient to affect the fungal metabolism in general while an increase of B can favor the formation of localized microenvironments and once they are colonized by fungi said magnetic field could also stimulate the fungal metabolism depending of the exposure time.

As for fungi, it was possible to observe similarity in their diversity and the predominant genera in the three geographic locations (RF of occurrence) were *Cladosporium* Link (100%), *Penicillium* Link (75%) and *Aspergillus*

 DOI: https://doi.org/10.30564/jasr.v3i3.2215

Link (75%).

These genera coincide with those reported previously in environmental studies in Havana [15, 43-45], also they prevailed in the supermarket Chong Chom in Thailand [46], in the room of the Terracotta Warriors in Mausoleum of the First Emperor Qin in China [47], in other archives, libraries and museums [48,49] as well as in the halls of Yale University (New Haven, Connecticut) where RF of occurrence of the genera *Cladosporium, Penicillium* and *Aspergillus* were 62, 40 and 26%, respectively [16]. These are considered normal contaminants of indoor environments and potentially allergenic, consistent with that reported previously [16].

According to these results it is suggested that it is common to find these fungal genera in indoor environments [36,44,49] and the predominance of one or the other depends on the climatic region and the specific sampling conditions [3]. In that sense, there was no significant difference ($p \leq 0.05$) for the counts of these genera among the three locations coinciding with that observed in houses located in the Havana center and other areas of Cuba [2,15,50-52].

When comparing the effect of the OMF on the microbial concentrations in the locals with the EG (EG-LI) and the TVs it was possible to obtain significant differences in presence of the TVs ($p \leq 0.05$). Table 4 shows the average of these values for the different study conditions.

A linear models were obtained for both cases that explains more than 85 and 89% ($R^2 = 0.85$ and 0.89) of the behavior of concentration filamentous fungi and TAM, respectively. The probability that the linear models do not satisfactorily explain the behavior of the response variables was very low, which is considered adequate. The following equation is obtained:

$RM = X_0 + X_1 \cdot A + X_2 \cdot B + X_3 \cdot C$

Where RM: microorganisms concentration in CFU/m^3 air; X_0: constant model; X_1, X_2 and X_3: regression coefficients; A: exposure time; B: distance to the TV; C: TV localization.

Table 4. Results obtained for fungi and yeast (FY) and total aerobic mesophilic (TAM) concentrations in each experimental condition according to the matrix experimental of design

No.	A: time of exposition (min)	B: distance to the TV (m)	C: Localization of TV	FY (CFU/m3)	TAM (CFU/m3)
1	60	1	AN	39	308
2	5	1	AN	79	111
3	60	0	EH	675	1062
4	15	0.5	AN	72	229
5	5	1	EH	39	144
6	30	0.5	EH	505	754
7	60	0	AN	177	668
8	60	0.5	AN	85	393
9	60	1	EH	197	301
10	60	1	EH	197	304
11	5	0.5	EH	662	1029
12	5	0	AN	111	498
13	5	0	AN	113	495
14	60	0	EH	675	1060
15	5	0	EH	491	832
16	60	0	AN	177	668
17	30	1	AN	38	216

Table 5 shows that fungal concentration was significant ($p \leq 0.05$) in relation to the factors distance to the appliances (B) and location (C), and it was non-significant ($p \geq 0.05$) for the exposure time (A). This result shows that the exposure time does not affect the final count value (positive sign of the coefficients). That is, only a larger number of colonies will be obtained by exposing the dishes for 10 or 30 min without affecting the profile of the response surface graphs obtained which coincide with those obtained in a previous similar study [20]. This shows that the location factor (C) only influences the variety of genera and species of microorganisms, not in the quantity [3, 20]. In this case was obtained a higher count of TAM (47.29 CFU/m^3) than FY (15.55 CFU/m^3) as these also can grow in the first group and can increase total count, as explained above. Such behavior is beneficial as it will contribute to a more representative air sampling. Negative signs of the coefficient B indicate that lower values of CFU/m^3 are achieved while the Petri dishes are located away from the appliances (Figure 1).

Table 5. Results of experiment design obtained from the averages actual count

Factor	Estimated Coefficients (CFU/m3)		p	
	FY	TAM	FY	TAM
Intercept	255.67	522.90	-	-
A (time of exposition)	15.55	47.29	0.6680	0.2971
B (distance to the TV)	-134.23	-272.26	0.0031	0.0001
C (localization of the TV)	-172.42	-156.78	0.0001	0.0017

Note:

FY: fungi and yeasts; TAM: total aerobic mesophilic.

At the EG-LI site, a statistically significant difference ($p \leq 0.05$) was observed for the FY concentration between the two periods of the year and the concentration was higher in the rainy season due to the increase in the relative humidity of the air, a factor that is very important for the sedimentation of fungal propagules. Among both microorganisms groups (TAM and FY) also there were statistically significant difference and the count of FY was higher than TAM in all samples.

The Figure 5 shows the distribution of microbial air

DOI: https://doi.org/10.30564/jasr.v3i3.2215

concentration at the EG-LI local and summarizes all information obtained during the study, and with it two factors were analyzed: operation of EG (turn on and turn off) and distance from the Petri dishes according theirs positions (0, 0.5 and 1 m). The formation of isolines (concentric rings) of more intense color centered surrounding the appliance is indicative of a higher microbial concentration in that area.

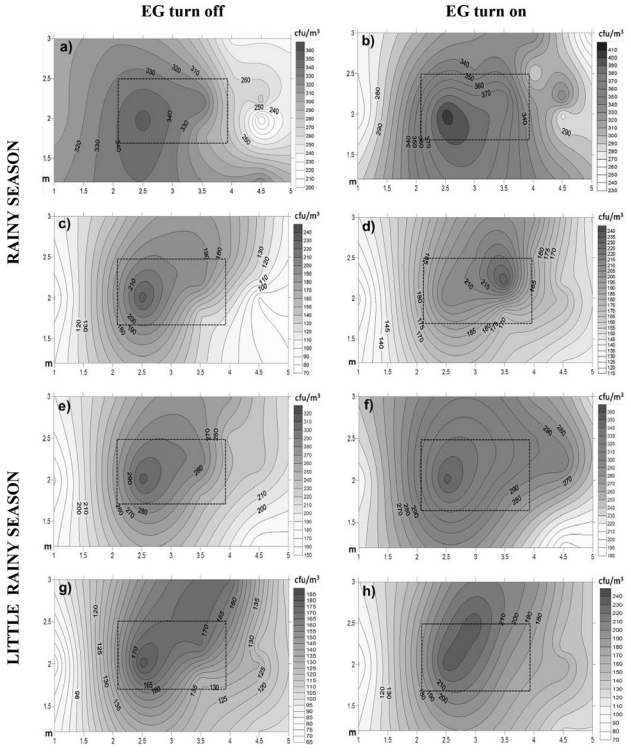

Figure 5. Distribution of microbiological concentration in the air (CFU /m3) on a local with the dimensions 6 x 4 x 3 m as well as an electrical generator (EG) of 47/51 kVA in different year seasons (rainy and little rainy seasons). Fungi - yeasts (a, b, e and f), total aerobic mesophilic (c, d, g and h). The rectangle of dotted line represents the area occupied by the EG in the room center

A similar behavior was observed regarding the increase of the air microbial concentration both in the experiments (EG turn on) and in the controls (EG turn off). This result evidences that there is influence of the equipment during its operation on the surrounding microbiota, probably due to the density of the magnetic field (B) existing in its vicinity or to the variation of aerodynamics that occurs (due to differences in temperature and relative humidity) when the EG is turn on. Although these variables were not controlled during the "in situ" experiment, their monitoring did not show statistically significant differences.

Figure 6 shows the relative density of each microbial group. Filamentous fungi outpaced the yeasts (Figure 6a) and among the bacteria, cocci predominated over the bacilli (Figure 6d). In the season of few rains the concentration of the filamentous fungi decreased but the yeasts increased (Figure 6c). It is important to highlight the low percentage detected of Gram negative bacteria (between 0 and 18%) as they are of great interest to public health because of its possible pathogenicity. In the rainy season (Figure 6e) the highest percentage of isolated bacteria were the Gram positive bacilli (59%) followed by the Gram positive cocci (29%). However, in the little rainy season no Gram negative cocci were found but the count of Gram negative bacteria was tripled (Figure 6f).

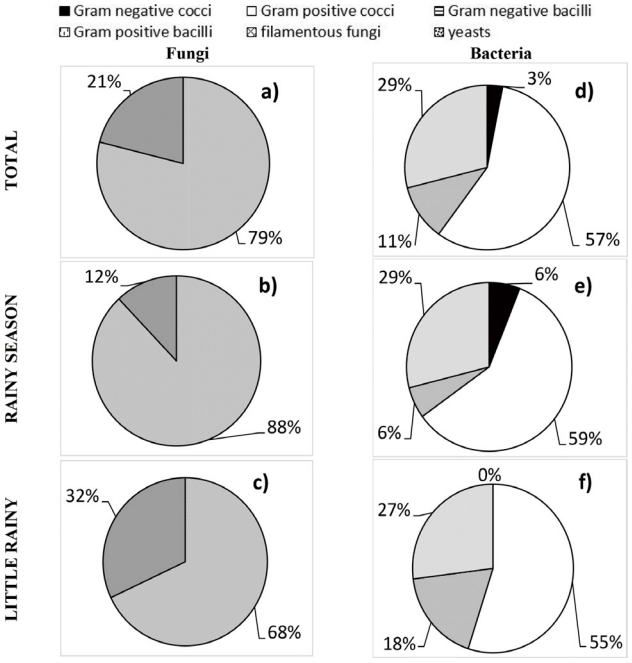

Figure 6. Relative density of the microbial concentration detected in the air of a local with dimensions 6 x 4 x 3 m as well as an electric generator of 47/51 kVA (turn on). Fungi and yeasts (a-c); bacteria (d-f) that are part of the total aerobic mesophilic group

A maximum colony count was obtained at the distance of 0 m and 1 h (60 min.) of exposure. As it is known within 3 cm of distance the televisions and computers generate a magnetic field of 50 and 30 μT, respectively [22]. With this result it is inferred that at densities less than 50 μT the microbial attraction towards the dishes is significantly lower than that observed in a similar environmental study with 10 mT [20]. In so far as Petri dishes are located away from the emitter center the incidence of the generated OMF density (B) by the household appliance decreases [22], so it is concluded that the value of B should be at least the double (100 μT), ie of the order of the militeslas (0.1 mT), to allow attraction of

 DOI: https://doi.org/10.30564/jasr.v3i3.2215

the existing aeromicrobiota in the indoor environment of any place.

4. Conclusions

The 60 Hz magnetic field generated by home appliances (0.01 to 50 μT) attracts many microbial colonies to the Petri dishes placed at 0.5 m of them, but these amounts are significantly lower than those attracted to 10 mT as observed in previous studies. Inhibition halos were formed by some bacterial colonies, a greater variety of filamentous fungi and a greater formation and excretion of pigments were observed in the Petri dishes that were located closer to the emitting source of OMF. A large variety of filamentous fungi was detected in the near of TVs and computers, which should be taken into account for the control of the microbiological quality of indoor air.

Acknowledgments

This investigation was made with the budget assigned by the Ministry of Science, Technology and Environment, Cuba (PCA- 2118025001) to execute the project to which belongs this result; hence the authors acknowledge this financial support.

References

[1] Bartra J. Mapa fúngico y estudio multicéntrico de sensibilización a hongos en Cataluña. Alergol Inmunol Clin., 2003, 18(Extraordinario Núm.3): 106-121.

[2] Díaz MJ, Gutiérrez A, González MC, Vidal G, Zaragoza RM, Calderón C. Caracterización aerobiológica de ambientes intramuro en presencia de cubiertas vegetales. Rev Int Contam Ambient., 2010, 26: 279-289.

[3] Rojas TI. Diversidad fúngica en ambientes interiores y exteriores en áreas urbanas de ciudad de La Habana. Doctoral Thesis in Biological Sciences. Faculty of Biology, Havana University, Cuba, 2011.

[4] Pasquarella C, Pitzurra O, Savino A. The index of microbial air contamination. J Hosp Infect., 2000, 46: 241-256.
DOI: 10.1053/jhin.2000.0820

[5] Martínez M, Fernández A, Molina E, García R. Grupos electrógenos y su impacto ambiental. Hig Sanid Ambient., 2007, 7: 217-221.

[6] Gómez A. Análisis de la eficacia de las medidas preventivas, correctoras y compensatorias de suelos, hidrología, ruido y patrimonio histórico para los proyectos de autovías en España. Thesis of Doctor in Sciences, 2007,
http://www.oa.upm.es/749/1/AdoracionGomezSanchez.pdf (Accessed July 24, 2014).

[7] Llamo HS. Influencia de la disposición de las fases de una línea doble circuito en su impacto ecológico. Campo magnético. Energética, 2006, 27(1): 3-8.

[8] Castro M, Perera RC, Pedrouzo J, Escobar A. Medición de campos electromagnéticos en redes de distribución: experiencias en Cuba. Energética, 2006, 27(1): 40-45.

[9] Curotto M, Magri S, Vidal M. Declaración de impacto ambiental de grupos electrógenos de respaldo minera Michilla, en Mejillones, Chile, 2008. (Accessed July 24, 2014):
http://www.e-seia.cl/archivos/R_01100715_SRK_MICHILLA_CONAMA.pdf

[10] Molina E, Cuba D. Contaminación del aire interior en un proyecto de viviendas con climatización centralizada. Rev Cubana Hig Epidemiol., 2006, 44(3): 12-16.

[11] Shelton BG, Kirkland KH, Flanders WD, Morris GK. Profiles of airborne fungi in buildings and outdoor environments in the United States. App Environ Microbiol., 2002, 68(4): 1743-1753.
DOI: 10.1128/AEM.68.4.1743–1753.2002

[12] Rodríguez GS, Sauri MR, Peniche I. Pacheco J. Ramírez JM. Aerotransportables viables en el área de tratamiento y disposición final de residuos sólidos municipales de Mérida, Yucatán. Ingeniería, 2005, 9(3): 19-29.

[13] Pasquarella C, Sansebastiano GE, Saccani E, Ugolotti M, Mariotti F, Boccuni C, Signerolli C, Fornari L, Alessandrini C, Albertini R. Proposal for an integrated approach to microbial environmental monitoring in cultural heritage: experience at the Correggio exhibition in Parma. Aerobiologia, 2011, 27: 203-211.
DOI: 10.1007/s10453-010-9189-4

[14] Frączek K, Górny RL. Microbial air quality at Szczawnica sanatorium, Poland. Ann Agric Environ Med., 2011, 18: 63-71.

[15] Rojas TI, Aira MJ, Batista A, Cruz LC, González S. Fungal biodeterioration in historic building of Havana (Cuba). Grana, 2012, 51: 44-51.
DOI: 10.1080/00173134.2011.643920

[16] Gent JF. Correlation of levels of house hold mold with respiratory symptoms in infants. Alergol Inmunol Clin., 2003, 18(Extraordinario Núm.3): 112-113.

[17] Zhdanova N, Tugay T, Dighton J, Zheltonozhsky V, Mcdermott P. Ionizing radiation attracts soil fungi. Mycol Res., 2004, 8: 1089-1096, DOI: 10.1017/S0953756204000966.

[18] Dadachova E, Casadevall A. Ionizing radiation: how fungi cope, adapt, and exploit with the help of melanin. Curr Opin Microbio., 2008, 11: 525-531.
DOI: 10.1016/j.mib.2008.09.013

DOI: https://doi.org/10.30564/jasr.v3i3.2215

[19] Dadachova E, Bryan RA, Huang X, Moadel T, Schweitzer AD. (2007) Ionizing radiation changes the electronic properties of melanin and enhances the growth of melanized fungi. Plos ONE, 2007, 2(5): e457.
DOI: 10.1371/journal.pone.0000457

[20] Anaya M, Castro M, Borrego SF, Cobo HC. Influencia del campo magnético sobre la calidad microbiológica del aire en interiores. Rev Soc Venez Microbio., 2015, 35: 47-52.

[21] Jamieson KS, Jamieson SS. Electromagnetic phenomena, microbial infection, charged oxygen and environmental air quality. In: Proceedings of VALDOR (Values in decisions on risk), pp. 281-283. Congrex Sweden AB/Informationsbolaget Nyberg & Co., Stockholm, Sweden, 14-18 May 2006.

[22] Henriquez D. Magnetismo, 2009, http://www.electromagnetismo221.blogspot.com, (Accessed Abril 15, 2012).

[23] Leach CM. Evidence for an electrostatic mechanism in spore discharge by Drechsrela turcica. Phytopathology, 1980, 70: 206-213.

[24] Shimizu K, Matsuda Y, Nonomura T, Ikeda H, Tamura N, Kusakari S. Dual protection of hydroponic tomatoes from rhizosphere pathogens Ralstonia solanacearum and Fusarium oxysporum f. sp. radicis-lycopersici and airborne conidia of Oidium neolycopersici with an ozone-generative electrostatic spore precipitator. Plant Pathol., 2007, 56: 987-997.
DOI: 10.1111/j.1365-3059.2007.01681.x

[25] Kakutani K, Matsuda Y, Kimbara J, Osamura K, Kusakari S. Practical application of an electric field screen to an exclusion of flying insect pests and airborne fungal conidia from greenhouses with a good air penetration. J Agric Sci., 2012, 4: 51-60.
DOI: 10.5539/jas.v4n5p51

[26] Takikawa Y, Matsuda Y, Nonomura T, Kakutani K, Kimbara J, Osamura K. Electrostatic guarding of bookshelves for mould-free preservation of valuable library books. Aerobiologia, 2014, 30: 435-444.
DOI: 10.1007/s10453-014-9340-8

[27] Bogomolova EV, Kirtsideli I. Airborne fungi in four stations of the St, Petersburg underground railway system. Int Biodeter Biodegr., 2009, 63: 156-160.
DOI: 10.1016/j.ibiod.2008.05.008

[28] Awad AH, Mawla HF. Sedimentation with the Omeliansky formula as an accepted technique for quantifying airborne fungi. Pol J Environ Stud., 2012, 21: 1539-1541.

[29] Borrego S, Lavin P, Perdomo I, Gómez de Saravia S, Guiamet, P. Determination of indoor air quality in archives and the biodeterioration of the documentary heritage. ISRN Microbiology, 2012.
DOI:10.5402/2012/680598

[30] Ellis MB. More Dematiaceous hyphomycetes. England: Commonwealth Mycological Institute, 1976.

[31] Barnett HL, Hunter BB. Illustrated genera of Imperfect fungi. 4th edn. Minneapolis: APS Press, 1998.

[32] Klich MA, Pitt JI. A laboratory guide to the common Aspergillus species and their teleomorphs, Australia: CSIRO, Division of Food Processing, 1994.

[33] Pitt JI. A laboratory guide to common Penicillium species. 3rd ed. Australia: CSIRO, Division of Food Processing, 2000.

[34] Abdel H, Ayesh AM, Abdel RM, Mawla HF. Fungi and some mycotoxins producing species in the air of soybean and cotton mills: a case study. Atmos Pollut Res., 2012, 3: 126-131.
DOI: 10.5094/APR.2012.012

[35] Anaya M, Borrego SF, Cobo HC, Valdés O, Molina, A. Aeromicobiota de un depósito de alimentos en La Habana, Cuba. Augmdomus, 2014, 6: 95-110.

[36] Anaya M, Borrego SF, Gámez E, Castro M, Molina A, Valdés O. Viable fungi in the air of indoor environments of the National Archive of the Republic of Cuba. Aerobiologia, 2016, 32: 513-527.
DOI: 10.1007/s10453-016-9429-3

[37] Terrés-Speziale AM. Manejo de la contaminación ambiental intramuros por medio de la generación de iones aéreos electronegativos. Rev Mex Patol Clin Med Lab., 2006, 53(1): 29-38.

[38] Chao HJ, Milton DK, Schwartz J, Burge HA. Dust-borne fungi in large office buildings. Mycopathologia, 2001, 154(2): 93-106.

[39] Karbowska-Berent J, Górny RL, Strzelczyk AB, Wlaz A. (2011) Airborne and dust borne microorganisms in selected Polish libraries and archives. Build Environ., 2011, 46(10): 1872-1879, DOI: 10.1016/j.buildenv.2011.03.007.

[40] Berg A, Berg H. Influence of ELF sinusoidal electromagnetic fields on proliferation and metabolite yield of fungi. Electromagn Biol Med., 2006, 25(1): 71-77.
DOI: 10.1080/15368370600581947
Gao M, Zhang J, Feng H. Extremely low frequency magnetic field effects on metabolite of Aspergillus niger. Bioelectromagnetics, 2011, 32(1): 73-78.
DOI: 10.1002/bem.20619

[42] Cordero RJB, Casadevall A. Functions of fungal melanin beyond virulence. Fungal Biol Rev., 2017, 31(2): 99-112.
DOI: 10.1016/j.fbr.2016.12.003

[43] Rodríguez JC. Evaluación aeromicrobiológica del depósito del Centro de Documentación del Museo Nacional de la Música de Cuba. Ge-conservación,

2016, (9): 117-126.

[44] Borrego S, Perdomo I. Airborne microorganisms cultivable on naturally ventilated document repositories of the National Archive of Cuba. Environ Sci Pollut Res., 2016, 23(4): 3747-3757.
DOI: 10.1007/s11356-015-5585-1

[45] Borrego S, Molina A. Fungal assessment on storerooms indoor environment in the National Museum of Fine Arts, Cuba. Air Qual Atmos Health., 2019, 12: 1373-1385.
DOI: 10.1007/s11869-019-00765-x

[46] Reanprayoon P, Yoonaiwong W. Airborne concentrations of bacteria and fungi in Thailand border marker. Aerobiologia, 2012, 28: 49-60.
DOI: 10.1007/s10453-011-9210-6

[47] Chen Y-P, Cui Y, Dong J-G. Variation of airborne bacteria and fungi at Emperor Qin's Terra-Cotta museum, Xi'an, China, during the "Oct. 1" Gold Week period of 2006. Environ Sci Pollut Res., 2010, 17: 478-485.
DOI: 10.1007/s11356-009-0161-1

[48] Pinheiro AC, Sequeira SO, Macedo MF. Fungi in archives, libraries, and museums: a review on paper conservation and human health. Crit Rev Microbiol., 2019.
DOI: 10.1080/1040841X.2019.1690420

[49] Borrego S, Molina A. Behavior of the cultivable airborne mycobiota in air-conditioned environments of three Havanan archives, Cuba. Journal of Atmospheric Science Research, 2020, 3(1): 16-28.
DOI: DOI: 10.30564/jasr.v3i1.1910

[50] Almaguer M, Rojas-Flores TI. Aeromicota viable de la atmósfera de La Habana, Cuba. Nova Acta Científica Compostelana (Bioloxía), 2013, 20: 35-45.

[51] Almaguer M, Aira MJ, Rodríguez-Rajo FJ, Rojas TI. Temporal dynamics of airborne fungi in Havana (Cuba) during dry and rainy seasons: influence of meteorological parameters. Int J Biometeorol, 2014, 58: 1459-1470.
DOI: 10.1007/s00484-013-0748-6

[52] Almaguer M, Aira MJ, Rodríguez-Rajo FJ, Fernandez-Gonzalez M, Rojas-Flores TI. Thirty-four identifiable airborne fungal spores at Havana, Cuba. Ann Agric Environ Med., 2015, 22: 220-225.
DOI: 10.5604/12321966.1152068

DOI: https://doi.org/10.30564/jasr.v3i3.2215

BILINGUAL PUBLISHING CO.
Pioneer of Global Academics Since 1984

Journal of Atmospheric Science Research
https://ojs.bilpublishing.com/index.php/jasr

REVIEW

Global Environmental Forecast and Roadmap Based on 420 kY of Paleoclimatology

Thomas F. Valone*

Integrity Research Institute, Beltsville, MD, USA

ARTICLE INFO

Article history
Received: 20 July 2020
Accepted: 28 July 2020
Published Online: 30 July 2020

Keywords:
Climate change
Thermal forcing
Temperature
Carbon dioxide
PETM
Carbon emissions
Carbon capture and storage
Climate Chart
paleoclimatology

ABSTRACT

As the world's population has tripled (3x) since 1950, with another 50% increase expected by 2100, global annual carbon dioxide emissions growth rate has quadrupled (4x) since 1950 and global energy demand has quintupled (5x), all in the same time period. This discontinuous combination can be called a "3-4-5 Triad" and the sudden acceleration in all three arenas is too stressful on the environment and the damaging effects will be felt globally for centuries to come unless drastic action is taken. More importantly, the energy demand at 5x is outstripping the other two. This clearly means that as the population explodes at 3x, the *emerging middle class wants almost twice as much as their usual share* as fossil-fueled generators spread around the globe and modern conveniences become more and more desirable. However, such energy demand at 5x is an artificial human need that is predicted by RMI.org to result in four to five billion new window-mounted air conditioners by 2050 that will add even more to the global warming caused by increasing atmospheric carbon. By an examination of paleoclimatology for the past 420,000 years, it is demonstrable that reducing the concentration of this single most prolific heat-trapping gas by geoengineering back to pre-industrial levels of less than 300 ppm can actually give humankind a collective control over the world's rapidly rising average global temperature and once more, a temperate climate to live in.

1. Introduction

The surprising rate of growth for our accelerating carbon dioxide emissions globally is dramatically shown in Figure 1 from a slide used in a 2019 slide presentation by this author (www.tinyurl.com/ValoneClimateSlideshow). Worldwide energy consumption reached a record 37 billion tons of CO_2 (*for a single year's total emission*) at the end of 2018, with the U.S, India, and China leading the increase. Note that only ten years before, the carbon dioxide annual emission rate was less than 30 gigatons. The total carbon emission growth rate in 2017 was only 1.7 percent while carbon growth for 2018 shown in Fig. 1 increased 2.7 percent (Figure 1), thus proving an accelerating trend that has no foreseeable "peak" in the growth rate or the actual magnitude of carbon dioxide annual emissions in the near future. As for China, coal accounts for about 60 percent of China's total energy consumption [1]. A major new paleoclimatology study also shows that current global

**Corresponding Author:*
Thomas F. Valone,
Integrity Research Institute, Beltsville, MD, USA;
Email: IRI@erols.com

 DOI: https://doi.org/10.30564/jasr.v3i3.2191

warming has reversed the past 6,500 years of global cooling [2].

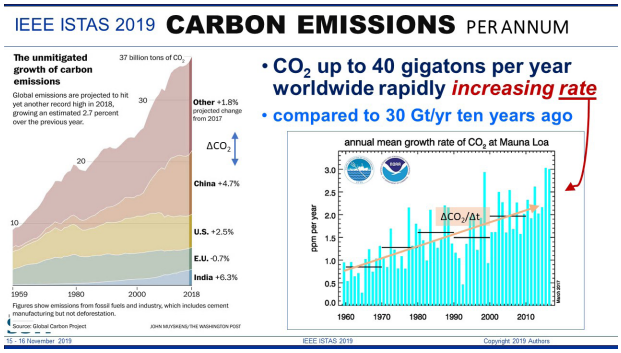

Figure 1. Annual global carbon emissions (left) and parts per million per year (right)

Global annual carbon dioxide emissions 1959-2018 as shown in Figure 1 started a new exponential surge upwards in 2017 [3]. Fossil fuel carbon emissions are now steadily increasing annually in several major countries in the world, which translates to the *rate of growth* having an upward slope, without a predictable peak, of either rate or magnitude, in the foreseeable future. Recent climate reports suggest a widely accepted range of one and a half (1.5°C) to two degrees (2°C) Celsius as an achievable global limit to climate change, which is unfounded, naïve, and basically misinformation. It is a direct contradiction to the observationally informed, published projections of climate science underlying global warming. A weather research station on Seymour Island in the Antarctic Peninsula, for example, registered a temperature of 69.3 degrees F (20.75 Celsius) on Feb. 9, 2020 according to Márcio Rocha Francelino, a professor at the Federal University of Vicosa in Brazil. The nearly 70-degree temperature is significantly higher than the 65-degree reading taken Feb. 6 at the Esperanza Base along Antarctica's Trinity Peninsula. The World Meteorological Organization (WMO) will decide whether it qualifies as the continent's hottest temperature on record. The new data came from a 12-year-old research station, used mainly for monitoring the layer of permafrost [4]. Furthermore, a Siberian town on the Arctic Circle hit 100 degrees F (38 degrees Celsius) near the end of June, 2020 setting a record. NOAA also reports that May, 2020 was the warmest May on record for Asia (NBC News, nbc.com).

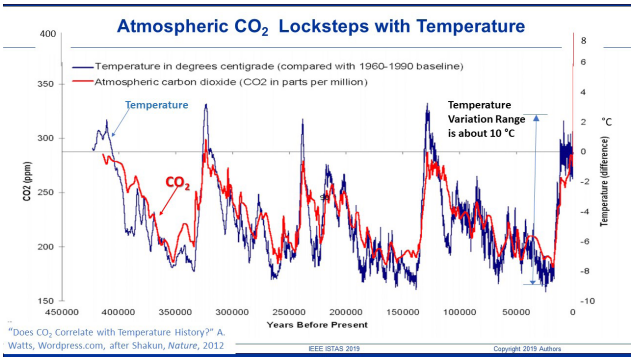

Figure 2. Carbon dioxide (ppm) levels and temperature (°C) for the past 400 kY

In Figure 2, we see a blue and red colored plot of the world average temperature and CO_2 data from air bubble analysis of the Vostok Station Antarctica ice core. In 1999, the Vostok ice core 420,000-year record of carbon dioxide was published by Petit et al [5]. *Exhibiting great stability, the CO_2 levels clearly have never exceeded 290 ppm worldwide even through four ice ages*. However, in the isolated monitoring station cited above for our modern, with our worldwide fossil fuel gluttony, the latest global carbon dioxide levels have now exceeded 410 ppm, with apparent universal disregard for the consequences. Clearly noticeable in Figure 2 is the tight correlation of temperature (blue graph) and carbon dioxide (red graph) for the past 420,000 years, which drives paleoclimatologists to reluctantly include the surprisingly high red line at the end (*present time on right side)* that has to be that high, to stay on the same scale and show the present world rise past 400 ppm of CO_2. Since the historic red and blue data lines show an actual climate record of the earth-atmospheric system, then the axis label of CO_2 concentration on the left necessarily correlates to the axis label of global temperature on the right, where the disturbing alignment near 8°C is registered in Figure 2. This dual graph begs the question, "Does CO_2 Correlate with Temperature History?" as Watts asks online at Wordpress.com after Shakun did so in Nature, 2012. The scientific answer has to be "yes" since humans have increased the level of CO_2 from the temperature-stabilizing 290 ppm up to 410 ppm presently, which equals a 43% increase in such a potent, heat-trapping substance surrounding our home. Any quantity in the earth system that balloons that much will always have a discontinuous impact and CO_2 definitely does. That is the only reason this article argues that geoengineering is required BEFORE the earth starts reaching the feared 6 to 8°C as it inevitably will in less than 100 years. An international consortium needs to perform hundred-

DOI: https://doi.org/10.30564/jasr.v3i3.2191

gigaton carbon capture and sequestration (CCS) *per year*, as soon as possible, in order to reduce the present level of carbon dioxide in the atmosphere back down toward 290 ppm or the survival of much of humankind is in question. However, the temperatures and humidity predicted for later this century are already here. Worse than that, the wet-bulb temperature (thermometer wrapped in a wet cloth) is closing in on 35°C (95°F), 25 to 30 times a year in several parts of the world already, which is the "survivability" wet-bulb temperature that defies sweating of even a healthy, young person, thus "endangering hundreds of millions of people" [6].

Jim Hansen's Table of Vostok data points for 400,000 years

Carbon dioxide p.p.m.	Average Earth temp. °C	Sea level meters
300	15.5	10
290	15.0	0
280	14.5	−10
270	14.0	−20
260	13.5	−30
250	13.0	−40
240	12.5	−50
230	12.0	−60
220	11.5	−70
210	11.0	−80
200	10.5	−90
190	10.0	−100
180	9.5	−110
170	9.0	−120

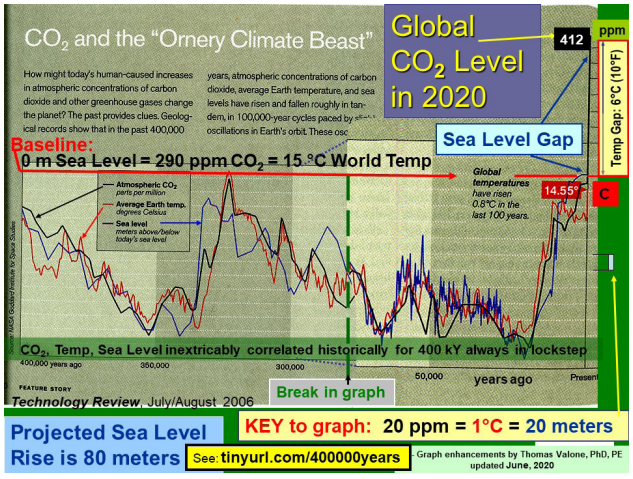

Figure 3. Author's summary of a predictive climate graph from Hansen (Tech. Rev., July, 2006)

In Figure 3, we have a condensed version of another 400,000 year old Vostok ice core record, along with scientific extrapolation of ancient sea levels, which in this case was published by famed climatologist James Hansen [7]. This author has annotated the beginning and end of his graph, as well as *included the data table* (on the left) to show the unexpectedly linear data that connects the three variables plotted (temperature, carbon dioxide, and sea level). Visiting www.tinyurl.com/400000years offers the reader a complete view of the entire 400,000 year history which is only partially shown and summarized in Figure 3. Note that the indicated "Temp Gap" or temperature gap is measured from the chosen historic maximum baseline is 15°C, which unfortunately is a contradiction in reality. Usually, any "baseline" in science is an average or a minimum from a time scale record. However, in this case, we have an extrema to deal with for a "baseline": the maximum value of temperature at 15°C and the maximum value of CO_2 for the past 400,000 years. Be that as it may, the prediction of a 6°C increase in temperature is arrived at quite simply. The temperature, carbon dioxide level, and sea level data clearly shown in the Table is easily translated into a simple equation seen in Figure 4. The equation is designed to allow anyone to compress the Table data into a formula that is easy to memorize. Thus, taking the values of 410 ppm (present) - 290 ppm (baseline) = 120 ppm, which equals the excess amount of CO_2 in the air. Dividing this excess by the 20 ppm discerned from the KEY of Figure 3 "per degree equivalent," the equation of Figure 4 makes it explicit so we convert to six (6°C), which must correspond to the equivalent, thermally connected system value of *temperature indebtedness*, that HAS to manifest as soon as the earth-atmosphere Gaia interaction allows. Stanford Research Institute suggests that a realistic extrapolation of the present temperature increasing data brings us to around 2100 for the extra 6°C to become the norm [8]. For humans, this expected scenario, with business as usual, will be an intolerable, inhospitable climate resulting in mass starvation, millions of deaths, desertification of vast tracts of land, including much of the mid-West United States, equatorial regions like the Arabian peninsula, with eventual tropical rainforest environments created in northerly climates, after the wildfires cease.

+/- 20 ppm = 1°C = 20 meters

Figure 4. The Hansen Equation linking global CO_2, temperature, and sea level

What may be the most reassuring part of the formula in Figure 4 is the +/- sign. As clearly seen in Figures 2 and 3, the response of the earth-atmosphere Gaia system to any change in global CO_2 levels entrains the other two to follow, with a corresponding delay. In other words, as humans wantonly pushed the CO_2 level rapidly above the 290 ppm baseline only in the past few decades with

DOI: https://doi.org/10.30564/jasr.v3i3.2191

very little delay in the rising temperature response to the heat-trapping gas increase, the reverse will also be seen to have a rapid effect worldwide. The reverse entails the world learning and implementing a lowering of the global level of carbon dioxide to 290 ppm, by CCS on an annual hundred-gigaton level, as renewable energy is gradually brought online.

While climatologists know the linear relationship between carbon dioxide levels and temperature exists, the United Nations Environmental Program (UNEP) and the International Panel on Climate Change (IPCC) among others are choosing to ignore the consequences of the present CO_2 excess, which now surpasses 43% of the maximum 290 ppm the earth has ever experienced in over 420,000 years. It is vital that the reader comprehends the blatant fact that the earth-atmosphere system, often referred to as "Gaia", is now indebted for 6 to 8 degrees C increase in temperature as shown in Figure 3 with the clarification of Figure 4. The trend graphs of Figure 5 tell the experts and any of the public who will take notice, the consequence of 400 ppm will manifest in approximately 80 years, by 2100 *compounded by the fact* that by then, we will most likely reach or surpass 800 ppm, unless something drastic is done to reduce the amount of carbon dioxide in the atmosphere globally. Note that this assessment of a predicted temperature rise of a 6 to 8 degrees C increase, will only become even more egregious and higher beyond 2100 unless carbon capture and storage (CCS) is instituted to bring down the concentration of CO_2 to pre-1950 levels of 290 ppm.

Looking at the sea level rise that the world is indebted for, we go back to the forsaken 370 ppm of CO_2 we saw in the air around the year 2006, when Hansen published his graph in Technology Review. We can take the rounded number 370-290 (zero value) = 80 ppm and divide by the 20 ppm from the formula into 80 ppm to get the disturbing number of 4 to multiply by 20 meters. Or we can just simply note that the numerical values of CO_2 and sea level change are the same, so sea level increase destined by Gaia is 80 meters, which is probably the maximum sea level increase possible. Any CO_2 value above the 30% increase from baseline, or about 370 ppm of that year, is hitting the ceiling of globally available ice since the major contributors to sea level rise are the landlocked glacier ice from Antarctica and Greenland. These huge glaciated island continents are the only two main landlocked glacier ice of frozen water on earth. Antarctica will contribute about 60 meters of sea level rise and Greenland is estimated to contribute about 10 meters which equals 70 meters, so even the 80-meter result may an overestimate.

2. Future Impact and Resolution

In Figure 5, we see the conclusion of the University of Washington (USA) which published a series of slides on the paleoclimatological implications of an 500-1000 ppm level of CO_2 that we are headed for by 2100 [9].

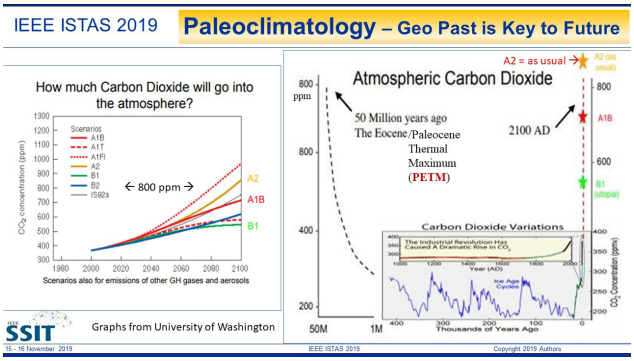

Figure 5. Computer projections for CO_2 at 2100 compared to the PETM with same levels of CO_2

The Eocene-Paleocene Thermal Maximum (PETM), which reached 800 ppm at its peak, is exactly what the experts predict for us even by the end of this century (2100). This is because of the clear trend in the exponential growth of CO_2 emissions worldwide, which is reflected in our Figures 1 and 2 CO_2 emissions graph with the rate of CO_2 emissions reaching about 3% presently in 2020, as well as the shocking projection of 800 ppm by 2100 as the "business as usual" most likely scenario for planet earth. Note that the earth-atmosphere system exhibits **a very short temporal feedback loop** between CO_2 average levels and global temperature: every report indicates hotter seasons than the previous ones as each year goes by. It can be estimated that there may be only a 20-year gap in the response curve of an increased (or decreased) global average level of CO_2 and the increase (or decrease) in worldwide average temperature. Therefore, more and more the primary recommendation of informed climatologists is that carbon capture and storage (CCS), also called "carbon sequestration", is the only hope for controlling the world's average temperature for the immediate and long-term future. The exciting reward is the quick response that the earth-atmosphere system will predictably offer, in only a few decades, to the responsible geoengineering of CCS on the hundreds of gigatons level that actually REDUCES the overall global average level of CO_2 by even thirty to fifty parts per million (ppm) perhaps.

DOI: https://doi.org/10.30564/jasr.v3i3.2191

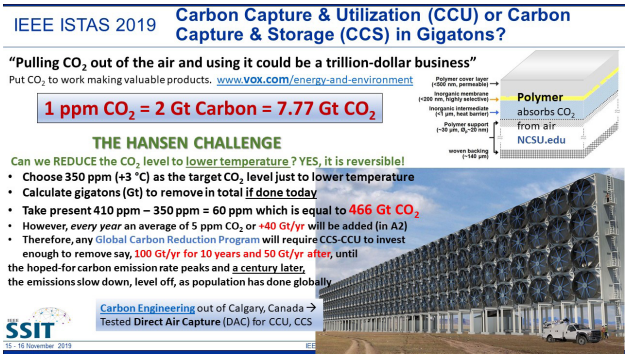

Figure 6. Proposed CCS for excess atmospheric CO_2 to restore preindustrial 290 ppm levels

In Figure 6, we delineate the relationship between the concentration of carbon dioxide and the amount 7.77 Gt (in gigatons), of the corresponding 1 ppm of CO_2. To explain, the main calculation driving the realistically predicted 6°C warming this century, by experts like Hansen and Caldeira, is the present 410 ppm of CO_2 in the air as compared to the 290 ppm that Dr. James Hansen and others regard as the BASELINE for the comfortable 15°C humans have enjoyed for centuries (see Figure 3, IRI 2020 Climate Chart based on Hansen's Vostok ice core graph). To summarize, 410 - 290 = 120 ppm and each part per million (ppm) equals 7.77 gigatons of CO_2. So when we multiply the 7.77 gigatons by the 41% increasing level of 120 ppm of heat-trapping CO_2, it yields **a scary 932 gigatons or almost one trillion tons of CO_2** that must be removed to restore our comfortable 15°C that everyone has enjoyed for centuries.

Late in 2020, Project Vesta plans to spread a green volcanic mineral known as olivine, ground down to the size of sand particles, across one of the world's beaches. The waves will further break down the highly reactive material, accelerating a series of chemical reactions that pull the greenhouse gas out of the air and lock it up in the shells and skeletons of mollusks and corals. This process, along with other forms of what's known as enhanced mineral weathering, could potentially store trillions of tons of carbon dioxide, according to a National Academies report last year. That is far more carbon dioxide than humans have pumped out since the start of the Industrial Revolution. Unlike methods of carbon removal that rely on soil, plants, and trees, it would be effectively permanent. Project Vesta at least believes it could be on the order of $10 per ton of stored carbon dioxide once it is done on a large scale [10].

The task of reducing the overall 410 ppm of CO_2 back down to 290 ppm, to completely and directly reverse the heat-trapping, global warming trend, is extremely important to comprehend and constitutes the main reason for publishing this information at this time, since the CCS responsibility it implies is staggering and unfortunately, increasing each year by more than 40 Gt. The amount of CCS needed is indeed huge but not impossible to engineer, only if a multi-nation conglomerate is formed in the next few years, if not sooner. Attention is directed to the equivalent formula in Figure 6 for converting the parts-per-million (ppm) amount of CO_2 to gigatons (Gt) of CO_2 for calculating the capture mode that can perhaps be used. This slide is taken from a presentation on this vital topic to an audience of professors and students at Tufts University in November, 2019 by this author, for the IEEE International Symposium on Technology And Society [11]. Note that in Figure 6, reference is made to "A2" which is found in Figure 5, which indicates a trend toward "business as usual" that so far, is the most reliable forecasting for the future unfortunately.

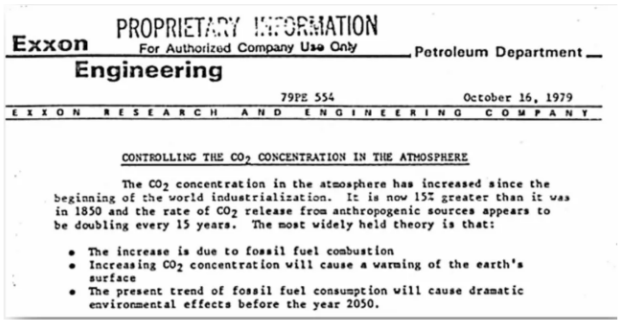
PROPRIETARY INFORMATION
For Authorized Company Use Only
Exxon Engineering
Petroleum Department
79PE 554
October 16, 1979
EXXON RESEARCH AND ENGINEERING COMPANY

CONTROLLING THE CO_2 CONCENTRATION IN THE ATMOSPHERE

The CO_2 concentration in the atmosphere has increased since the beginning of the world industrialization. It is now 15% greater than it was in 1850 and the rate of CO_2 release from anthropogenic sources appears to be doubling every 15 years. The most widely held theory is that:

- The increase is due to fossil fuel combustion
- Increasing CO_2 concentration will cause a warming of the earth's surface
- The present trend of fossil fuel consumption will cause dramatic environmental effects before the year 2050.

Figure 7. Surprising Exxon 1979 memo linking fossil fuels to atmospheric CO_2

Many states in America are now suing oil companies for fraud today (Minnesota, Rhode Island, Massachusetts, New York, Washington DC, etc.) since memos stating that "controlling the CO_2 concentration in the atmosphere" have been directly connected to fossil fuel combustion and warming of the earth, since at least 1979 (Figure 7) [12]. If oil companies are acutely aware of the long-term health and environmental damage they are doing, with no clear resolution in sight, what are municipalities and governments supposed to do? The only rational hope is to take the lessons learned from the COVID-19 crisis and start international networking on a grand scale, using the worldwide response to the virus as a template that works. Creating a sense of urgency and even emergency is the beginning to cause action.

DOI: https://doi.org/10.30564/jasr.v3i3.2191

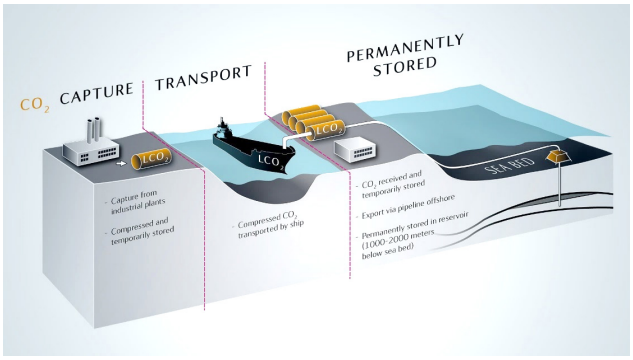

Figure 8. Simple diagram illustrating a method for successful CCS

There is presently in the latter part of 2020, a steady public shift away from outright climate denial, as exhibited by rank-and-file members of the U.S. Republican Party, as evidence that attitudes can move toward action, no matter how meager. Now that the unconscious repression of the truth is finally dissolving, an avalanche of action could soon follow. As Rear Admiral David Titley once said, "We may be much closer to catastrophic success right now. Things can change, and not always for the worse. They can change for the better. It can happen very, very quickly" [13].

To happen very quickly, a CCS process like Project Vesta or Project Northern Lights [14] (Figure 8) would have to be ramped up to the hundred-gigaton level indicated above. It also requires a cooperative international fund donation of at least $1 to $10 trillion, if and only if the estimated price per ton can be brought down, through government subsidies perhaps, to $1 to $10 per ton. Then and only then, the excess, *global warming driver* of 932 gigatons of CO_2 can be rapidly (over a ten-year period in the least) captured and stored (see Figures 6-9) with that total investment. Then, within only a few decades, the response of the earth-atmosphere Gaia system will joyfully reward us with cooler temperatures back down to pre-industrial levels, besides helping to stop glacial melting and perhaps instead, refreeze the glaciers. We see in Figure 9 a third process, from the Carbon Engineering company plan for a grand scale removal of one megaton per year of CO_2 from the atmosphere (artist drawing of their fan-driven assembly is in Figure 6), using a potassium hydroxide sorbent coupled with a calcium caustic recovery loop seen in the process diagram [15].

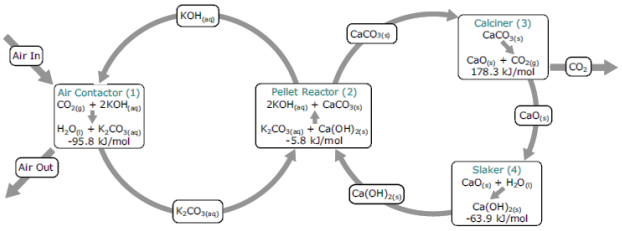

Figure 9. Industrial process diagram for removing one megaton of CO_2 per year from air

The lowest cost estimate from the article about Carbon Engineering's plan, in today's Canadian dollars, is slightly less than $100/ton of processed CO_2 which is a prohibitive price for large scale implementation in the gigaton range and beyond at the present time. Their industrial process, being the first to provide complete details for implementing large scale direct air capture (DAC) of atmospheric CO_2, serves two purposes. First, the process can assist in making carbon neutral hydrocarbon fuels, especially if the process is solar-driven. Even the aviation industry can decarbonize in this way with DAC-CO_2 and electrolytic hydrogen to make high-energy-density jet fuel. Second, by adding storage (sequestration) DAC enables a quantity of carbon removal from the atmosphere permanently. To help further public research in this vital area, an exhaustive set of references is provided, from 2004 to the present, on capturing and removing CO_2 from ambient air, many of which provide open access to their article [16-27].

It is genuinely hoped that this information will be widely distributed to decision-makers, climatologists, and billionaires worldwide, telling them that global warming is reversible, and CCS action needs to be taken sooner, rather than later, to avert skyrocketing annual increases in costs, besides severe biological impacts by 2100 of heat, drought, crop failure, hunger, migratory unrest, strife, border wars, and widespread death and disease that such a high, global temperature increase of 6 to 8°C within 80 to 100 years entails.

References

[1] Dennis, Brady, Chris Mooney. "We are in trouble". Global carbon emissions reached a record high in 2018. Washington Post, 2018.

[2] Northern Arizona University. Major new paleoclimatology study shows global warming has upended 6,500 years of cooling. Phys.org, 2020. https://phys.org/news/2020-06-major-paleoclimatology-global-upended-years.html

[3] Muyskens, John. The unmitigated growth of carbon

DOI: https://doi.org/10.30564/jasr.v3i3.2191

emissions. source: Global Carbon Project, Washington Post, 2018.

[4] Freedman, Andrew. Temperature in Antarctica soars to near 70 degrees, appearing to topple continental record set days earlier. Washington Post, February 14, 2019.

[5] Petit J.R., Jouzel J., Raynaud D., Barkov N.I., Barnola J.M., et al. Climate and Atmospheric History of the Past 420,000 years from the Vostok Ice Core, Antarctica. Nature, 1999, 399: 429-436.

[6] Lambert, Jonathan.Deadly heat and humidity are here. Science News, 2020.
www.sciencenews.org

[7] Bowen, Mark. The Messenger. July 1, 2006, MIT Technology Review, https://www.technologyreview.com/s/406011/the-messenger / with David Talbot, "CO2 and the Ornery Climate Beast Chart", NASA Goddard Institute of Space Studies, Technology Review, 2006: 40-41.
https://s3.amazonaws.com/files.technologyreview.com/p/pub/legacy/articlefiles/climatechart.pdf

[8] Brown, Patrick, Ken Caldeira. Greater future global warming inferred from Earth's recent energy budget. Nature, 2017, 552: 45-50.

[9] Projections of Climate Change: 2100 and Beyond. part 2, University of Washington.
https://atmos.uw.edu/academics/classes/2011Q1/101/Climate_Change_2011_part2.pdf

[10] Temple, James. How green sand could capture billions of tons of carbon dioxide. MIT Technology Review, 2020.
https://www.technologyreview.com/2020/06/22/1004218/how-green-sand-could-capture-billions-of-tons-of-carbon-dioxide

[11] Valone, Thomas, Jacqueline Panting. Quantitative Carbon Dioxide, Temperature, and Sea Level Relation for the Future of Terrestrial Fossil-Fueled Technology, An Accurate Predictive Model Based on Vostok 420 kY Historical Record. IEEE International Symposium on Technology and Society (ISTAS) Proceedings, 15-16 November 2019, School of Engineering, Tufts University, Medford MA.
https://www.slideshare.net/ThomasValonePhD/valone-ieee-istas2019ppt-ver4-with-extra-slide-with-links-at-end

[12] Savage, Karen. Minnesota Sues Fossil Fuel Industry for Climate Fraud. The Climate Docket, 2020.
https://www.climatedocket.com/2020/06/24/minnesota-climate-lawsuit-exxon-koch-api

[13] Holthaus, Eric. The Future Earth: A Radical Vision for What's Possible in the Age of Warming, HarperOne, HarperCollins Publishers, 2020.

[14] Rathi, Akshat. Norway's $2.6 Billion Green Bet Could Help the Whole Planet: A carbon capture project aims to make Norway the hub for other countries to bury their emissions. Bloomberg Green, 2020.
https://www.bloomberg.com/news/articles/2020-06-30/norway-carbon-capture-plan-aims-to-let-countries-bury-emissions

[15] Keith, David W. A Process for Capturing CO2 from the Atmosphere. Joule, 2018, 2: 1573-1594. (open access)
https://doi.org/10.1016/j.joule.2018.05.006

[16] Socolow, R. et al. Direct Air Capture of CO2 with Chemicals: A Technology Assessment for the APS Panel on Public Affairs. 2011. (open access)
https://infoscience.epfl.ch/record/200555/files/dac2011.pdf

[17] Lackner, Klaus S. The urgency of the development of CO2 capture from ambient air. PNAS, 2012, 109(33): 13156-13162.
https://doi.org/10.1073/pnas.1108765109

[18] Sanz-Perez, Eloy S. et al. Direct Capture of CO2 from Ambient Air. Chemical Reviews, 2016, 116(19): 11840-11876.
https://pubs.acs.org/doi/10.1021/acs.chemrev.6b00173

[19] Martin D. et al. Carbon Dioxide Removal Options: A Literature Review Identifying Carbon Removal Potentials and Costs. University of Michigan Energy Institute, 2018. (Available at:)
http://energy.umich.edu/research/publications/carbon-dioxide-removal-options-literature-review-identifying-carbon-removal

[20] Wilcox J. et al. Assessment of reasonable opportunities for direct air capture. Environ. Res. Lett. 2017, 12: 065001. (open access)
https://iopscience.iop.org/article/10.1088/1748-9326/aa6de5
Mazzotti M. et al. Direct air capture of CO2 with chemicals: optimization of a two-loop hydroxide carbonate system using a countercurrent air-liquid contactor. Climate Change. 2013, 118: 119-135. (open access)
https://link.springer.com/article/10.1007/s10584-012-0679-y

[21] Stolaroff J.K. et al. Carbon dioxide capture from atmospheric air using sodium hydroxide spray. Environ. Sci. Technol. 2008, 42: 2728-2735.
https://pubs.acs.org/doi/10.1021/es702607w

[22] Zeman F. Reducing the cost of Ca-based direct air capture of CO2. Environ. Sci. Technol. 2014, 48: 11730-11735.
https://pubs.acs.org/doi/10.1021/es502887y

 DOI: https://doi.org/10.30564/jasr.v3i3.2191

[23] Burhenne L. et al. Characterization of reactive CaCO3 crystallization in a fluidized bed reactor as a central process of direct air capture. J. Environ. Chem. Eng. 2017, 5: 5968-5977. https://www.sciencedirect.com/science/article/abs/pii/S2213343717305481

[24] Holmes G. et al. An air-liquid contactor for large-scale capture of CO2 from air. Philos. Trans. A Math. Phys. Eng. Sci. 2012, 370: 4380-4403. (open access) https://royalsocietypublishing.org/doi/10.1098/rsta.2012.0137

[25] Holmes G. et al. Outdoor prototype results for direct atmospheric capture of carbon dioxide. Energy Procedia. 2013: 6079-6095. https://doi.org/10.1016/j.egypro.2013.06.537

[26] Smith P. et al. Biophysical and economic limits to negative CO2 emissions. Nat. Clim. Change. 2016; 6: 42-50.

[27] https://www.nature.com/articles/nclimate2870. Accessed by: https://kopernio.com/viewer?doi=10.1038/nclimate2870&route=1

DOI: https://doi.org/10.30564/jasr.v3i3.2191

Author Guidelines

This document provides some guidelines to authors for submission in order to work towards a seamless submission process. While complete adherence to the following guidelines is not enforced, authors should note that following through with the guidelines will be helpful in expediting the copyediting and proofreading processes, and allow for improved readability during the review process.

Ⅰ. Format

- Program: Microsoft Word (preferred)
- Font: Times New Roman
- Size: 12
- Style: Normal
- Paragraph: Justified
- Required Documents

Ⅱ. Cover Letter

All articles should include a cover letter as a separate document.

The cover letter should include:

- Names and affiliation of author(s)

The corresponding author should be identified.

Eg. Department, University, Province/City/State, Postal Code, Country

- A brief description of the novelty and importance of the findings detailed in the paper

Declaration

v Conflict of Interest

Examples of conflicts of interest include (but are not limited to):

- Research grants
- Honoria
- Employment or consultation
- Project sponsors
- Author’s position on advisory boards or board of directors/management relationships
- Multiple affiliation
- Other financial relationships/support
- Informed Consent

This section confirms that written consent was obtained from all participants prior to the study.

- Ethical Approval

Eg. The paper received the ethical approval of XXX Ethics Committee.

- Trial Registration

Eg. Name of Trial Registry: Trial Registration Number

- Contributorship

The role(s) that each author undertook should be reflected in this section. This section affirms that each credited author has had a significant contribution to the article.

1. Main Manuscript
2. Reference List
3. Supplementary Data/Information

Supplementary figures, small tables, text etc.

As supplementary data/information is not copyedited/proofread, kindly ensure that the section is free from errors, and is presented clearly.

Ⅲ. Abstract

A general introduction to the research topic of the paper should be provided, along with a brief summary of its main results and implications. Kindly ensure the abstract is self-contained and remains readable to a wider audience. The abstract should also be kept to a maximum of 200 words.

Authors should also include 5-8 keywords after the abstract, separated by a semi-colon, avoiding the words already used in the title of the article.

Abstract and keywords should be reflected as font size 14.

Ⅳ. Title

The title should not exceed 50 words. Authors are encouraged to keep their titles succinct and relevant.

Titles should be reflected as font size 26, and in bold type.

Ⅳ. Section Headings

Section headings, sub-headings, and sub-subheadings should be differentiated by font size.

Section Headings: Font size 22, bold type

Sub-Headings: Font size 16, bold type

Sub-Subheadings: Font size 14, bold type

Main Manuscript Outline

Ⅴ. Introduction

The introduction should highlight the significance of the research conducted, in particular, in relation to current state of research in the field. A clear research objective should be conveyed within a single sentence.

Ⅵ. Methodology/Methods

In this section, the methods used to obtain the results in the paper should be clearly elucidated. This allows readers to be able to replicate the study in the future. Authors should ensure that any references made to other research or experiments should be clearly cited.

Ⅶ. Results

In this section, the results of experiments conducted should be detailed. The results should not be discussed at length in

this section. Alternatively, Results and Discussion can also be combined to a single section.

Ⅷ. Discussion

In this section, the results of the experiments conducted can be discussed in detail. Authors should discuss the direct and indirect implications of their findings, and also discuss if the results obtain reflect the current state of research in the field. Applications for the research should be discussed in this section. Suggestions for future research can also be discussed in this section.

Ⅸ. Conclusion

This section offers closure for the paper. An effective conclusion will need to sum up the principal findings of the papers, and its implications for further research.

Ⅹ. References

References should be included as a separate page from the main manuscript. For parts of the manuscript that have referenced a particular source, a superscript (ie. [x]) should be included next to the referenced text.

[x] refers to the allocated number of the source under the Reference List (eg. [1], [2], [3])

In the References section, the corresponding source should be referenced as:

[x] Author(s). Article Title [Publication Type]. Journal Name, Vol. No., Issue No.: Page numbers. (DOI number)

Ⅺ. Glossary of Publication Type

J = Journal/Magazine

M = Monograph/Book

C = (Article) Collection

D = Dissertation/Thesis

P = Patent

S = Standards

N = Newspapers

R = Reports

Kindly note that the order of appearance of the referenced source should follow its order of appearance in the main manuscript.

Graphs, Figures, Tables, and Equations

Graphs, figures and tables should be labelled closely below it and aligned to the center. Each data presentation type should be labelled as Graph, Figure, or Table, and its sequence should be in running order, separate from each other.

Equations should be aligned to the left, and numbered with in running order with its number in parenthesis (aligned right).

Ⅻ. Others

Conflicts of interest, acknowledgements, and publication ethics should also be declared in the final version of the manuscript. Instructions have been provided as its counterpart under Cover Letter.

BILINGUAL PUBLISHING CO.
Pioneer of Global Academics Since 1984

Journal of Atmospheric Science Research

Aims and Scope

Journal of Atmospheric Science Research publishes original research papers that offers a rapid review and publication that freely disseminates research findings in areas of Remote Sensing, Weather Extremes, Air Pollution, Satellite Meteorology and more. The Journal focuses on innovations of research methods at all stages and is committed to providing theoretical and practical experience for all those who are involved in these fields.

Journal of Atmospheric Science Research aims to discover innovative methods, theories and studies in all aspects of Atmospheric Science by publishing original articles, case studies and comprehensive reviews.

The scope of the papers in this journal includes, but is not limited to:

- Remote Sensing
- Climate Dynamics
- Air Chemistry
- Hydrological Cycle
- Satellite Meteorology
- Ocean Dynamics
- Climate Change
- Weather Extremes
- Air Pollution
- Weather and Climate Prediction
- Climate Variability

Bilingual Publishing Co. (BPC)

Tel:+65 65881289

E-mail:contact@bilpublishing.com

Website:www.bilpublishing.com

About the Publisher

Bilingual Publishing Co. (BPC) is an international publisher of online, open access and scholarly peer-reviewed journals covering a wide range of academic disciplines including science, technology, medicine, engineering, education and social science. Reflecting the latest research from a broad sweep of subjects, our content is accessible world-wide——both in print and online.

BPC aims to provide an analytics as well as platform for information exchange and discussion that help organizations and professionals in advancing society for the betterment of mankind. BPC hopes to be indexed by well-known databases in order to expand its reach to the science community, and eventually grow to be a reputable publisher recognized by scholars and researchers around the world.

BPC adopts the Open Journal Systems, see on ojs.bilpublishing.com

Database Inclusion

Asia & Pacific Science Citation Index

Creative Commons

China National Knowledge Infrastructure

Google Scholar

Crossref

MyScienceWork

BILINGUAL
PUBLISHING CO.
Pioneer of Global Academics Since 1984

Tel:+65 65881289
E-mail:contact@bilpublishing.com
Website:www.bilpublishing.com